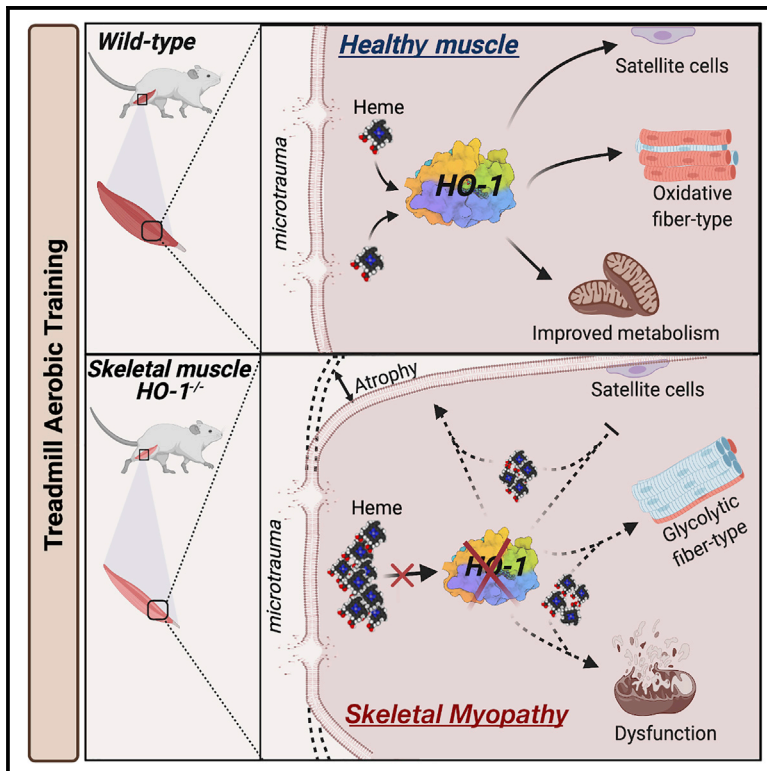


# Skeletal muscle heme oxygenase-1 activity regulates aerobic capacity

## Graphical abstract



## Authors

Rodrigo W. Alves de Souza, David Gallo, Ghee Rye Lee, ..., Ulrik Wisløff, Patricia C. Brum, Leo E. Otterbein

## Correspondence

lotterbe@bidmc.harvard.edu

## In brief

Alves de Souza et al. show that deficiency in the heme-degrading enzyme heme oxygenase-1 in skeletal muscle results in atrophy, mitochondrial dysfunction, and a profound inability to adapt to exercise. Heme metabolism is an essential pathway necessary for developing and maintaining exercise capacity, tissue damage control, and muscle health.

## Highlights

- Aerobic exercise increases circulating free heme due to skeletal muscle microtrauma
- Hemopexin-null mice show higher heme levels but no difference in running capacity
- Skeletal muscle lacking HO-1 has defective mitochondria and a fatigue-prone phenotype
- HO-1 is required to maintain skeletal muscle health during aerobic training



## Article

# Skeletal muscle heme oxygenase-1 activity regulates aerobic capacity

Rodrigo W. Alves de Souza,<sup>1,7</sup> David Gallo,<sup>1</sup> Ghee Rye Lee,<sup>1</sup> Eri Katsuyama,<sup>2</sup> Alexa Schaufler,<sup>1</sup> Janick Weber,<sup>1</sup> Eva Csizmadia,<sup>1</sup> George C. Tsokos,<sup>2</sup> Lauren G. Koch,<sup>3</sup> Steven L. Britton,<sup>4,5</sup> Ulrik Wisløff,<sup>6</sup> Patricia C. Brum,<sup>7,8</sup> and Leo E. Otterbein<sup>1,8,9,\*</sup>

<sup>1</sup>Department of Surgery, Beth Israel Deaconess Medical Center, Harvard Medical School, Boston, MA 02115, USA

<sup>2</sup>Department of Medicine, Beth Israel Deaconess Medical Center, Harvard Medical School, Boston, MA 02115, USA

<sup>3</sup>Department of Physiology & Pharmacology, The University of Toledo, Toledo, OH 43606, USA

<sup>4</sup>Department of Anesthesiology, University of Michigan, Ann Arbor, MI 48109, USA

<sup>5</sup>Department of Molecular and Integrative Physiology, University of Michigan, Ann Arbor, MI 48109, USA

<sup>6</sup>K.G. Jebsen Center of Exercise in Medicine, Department of Circulation and Medical Imaging, Norwegian University of Science and Technology, Trondheim 7491, Norway

<sup>7</sup>School of Physical Education and Sport, University of São Paulo, São Paulo 05508030, Brazil

<sup>8</sup>These authors contributed equally

<sup>9</sup>Lead contact

\*Correspondence: [lotterbe@bidmc.harvard.edu](mailto:lotterbe@bidmc.harvard.edu)

<https://doi.org/10.1016/j.celrep.2021.109018>

## SUMMARY

Physical exercise has profound effects on quality of life and susceptibility to chronic disease; however, the regulation of skeletal muscle function at the molecular level after exercise remains unclear. We tested the hypothesis that the benefits of exercise on muscle function are linked partly to microtraumatic events that result in accumulation of circulating heme. Effective metabolism of heme is controlled by Heme Oxygenase-1 (HO-1, *Hmox1*), and we find that mouse skeletal muscle-specific HO-1 deletion (*Tam-Cre-HSA-Hmox1<sup>fl/fl</sup>*) shifts the proportion of muscle fibers from type IIA to type IIB concomitant with a disruption in mitochondrial content and function. In addition to a significant impairment in running performance and response to exercise training, *Tam-Cre-HSA-Hmox1<sup>fl/fl</sup>* mice show remarkable muscle atrophy compared to *Hmox1<sup>fl/fl</sup>* controls. Collectively, these data define a role for heme and HO-1 as central regulators in the physiologic response of skeletal muscle to exercise.

## INTRODUCTION

The benefit of physical exercise profoundly affects the quality of life and prevention of chronic diseases for millions of people worldwide. There is growing interest in identifying molecular events associated with physical exercise that affect fitness and carry health benefits (Gabriel and Zierath, 2017). Physical exercise is a systemic process that relies on the coordination of cell pathways in different tissues and organs. During physical exercise, muscle microtrauma and heme release from intracellular stores has been observed in a process described for more than 50 years (Gilligan et al., 1943; Sartorelli and Fulco, 2004). During such events, free hemoproteins are released into the extracellular space; once oxidized, they release heme and, as such, fall into the category of danger-associated molecular patterns (DAMPs). DAMPs at low levels are powerful signaling molecules in response to acute cellular stress but are considered toxic in high levels (Gozzelino et al., 2010; Immenschuh et al., 2017). Therefore, the amount of free heme is tightly regulated so as to maintain cellular homeostasis and avoid progression to pathophysiology while driving the activation of specific cell-signaling events.

Heme metabolism is controlled by two physiologic systems that are interdependent of each other. Hemopexin (Hpx) is a scavenger protein in serum that possesses the highest binding affinity for free heme (Tolosano and Altruda, 2002). Upon binding of heme, Hpx is internalized via CD91/LRP1-mediated receptor endocytosis by most cells (Hvidberg et al., 2005). Second, and perhaps more importantly, increases in intracellular heme rapidly induce expression of heme oxygenase-1 (HO-1). HO-1 is powerfully cytoprotective through increased enzymatic degradation of heme into three bioactive molecules: carbon monoxide (CO), iron, and biliverdin (Otterbein et al., 2003). Among all known mechanisms of cytoprotection, the heme degradation pathway is the only catalytic process that allows removal of heme released from damaged cells and tissues, especially skeletal muscle, in which there is an enormous concentration confined within myoglobin (Neya, 2013). We have previously reported that HO-1 and its product CO are potentially protective in muscular dystrophy (Chan et al., 2016). Moreover, studies have shown that HO-1 is a potent regulator of differentiation of muscle progenitors into myocytes and myotubes *in vitro* (Pilegaard et al., 2000; Ren et al., 2016). However, despite the evidence that HO-1 is induced in cardiac, smooth, and skeletal muscle after



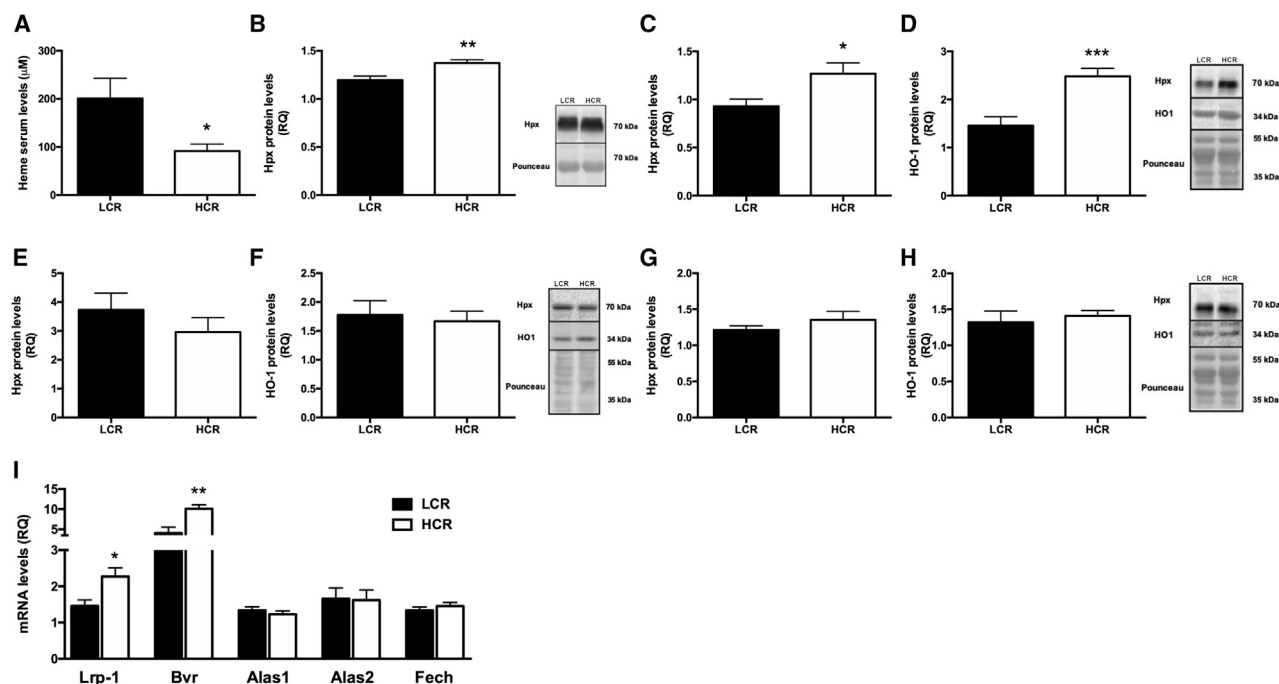


**Figure 1. Effects of low (LCR) and high (HCR) intrinsic running capacity on heme processing**

(A and B) Serum heme and Hpx levels comparing LCR and HCR rats.

(C and D) Hpx and HO-1 expression in plantaris skeletal muscle.

(E–H) Hpx and HO-1 expression in liver and heart, respectively, comparing LCR and HCR animals.

(I) Gene expression in plantaris muscle comparing LCR and HCR rats.

Results are expressed as mean  $\pm$  SEM. \* $p < 0.05$ , \*\* $p < 0.01$ , \*\*\* $p < 0.001$ ;  $n = 10/\text{group}$ .

exercise, no study has comprehensively investigated the contribution of heme degradation on skeletal muscle biochemistry and physiology as it relates to exercise performance and associated health benefits.

Here, we tested the hypothesis that heme metabolism is critical in skeletal muscle cell recovery and maintenance of function after aerobic exercise. We show that in the absence of Hpx, both untrained and trained mice exhibit no muscle deficits. In contrast, mice lacking HO-1 selectively in skeletal muscle fibers show dramatic structural and functional remodeling toward a fast and more fatigue-prone phenotype. We discovered that loss of HO-1 within muscle fibers impaired the benefits of aerobic exercise training (TR) and altered the muscle phenotype within weeks of deletion, driven largely by changes in metabolism and mitochondrial bioenergetics. Collectively, this study provides insights into the role of heme flux as an essential pathway necessary for developing and maintaining exercise capacity and muscle physiology.

## RESULTS

### Intrinsic high aerobic capacity improves heme metabolism in rats

High aerobic capacity (i.e., the capacity to use oxygen), is associated with metabolic benefits, cardiovascular protection, and longevity, which are hallmarks of HO-1 activity (Booth et al., 2012; Kokkinos et al., 2008). To investigate the role of heme on

intrinsic aerobic capacities, we first measured the total amount of heme and Hpx content in serum of selected cohorts of rats classified as having low or high intrinsic running capacity (LCR/HCR). We demonstrated previously that Hpx is one of the top oxidized proteins in HCR runners using proteomics (Koch and Britton, 2001; Souza et al., 2018). We found a significant reduction in heme levels concomitant with an increase in Hpx levels in HCR compared with LCR runners (Figures 1A and 1B). This corresponded with an increase in Hpx and HO-1 expression in skeletal muscle, neither of which were changed in the liver or heart (Figures 1C–1H). In addition, we observed a significant increase in expression of the heme-Hpx receptor LRP-1/CD91, as well as biliverdin reductase (BVR) expression in plantaris muscle, indicating that heme is likely internalized and fully metabolized by HO-1 and BVR to its end product bilirubin (Figure 1I). Gene expression analysis of transcripts involved in intracellular heme biosynthesis, including  $\delta$ -aminolevulinic acid (ALA) and ferrochelatase (Fech), showed no differences in either Alas1/2 or Fech in skeletal muscle when comparing HCR to LCR animals (Figure 1I). Collectively, these data partly associate intrinsic aerobic capacity with overall metabolic health and heme regulation.

### Aerobic exercise increases heme release in mice

The preceding results comparing HCR/LCR animals directed us to investigate further the effects of aerobic exercise on heme processing. First, we examined heme flux over time using an acute aerobic exercise protocol. Immediately after an exercise

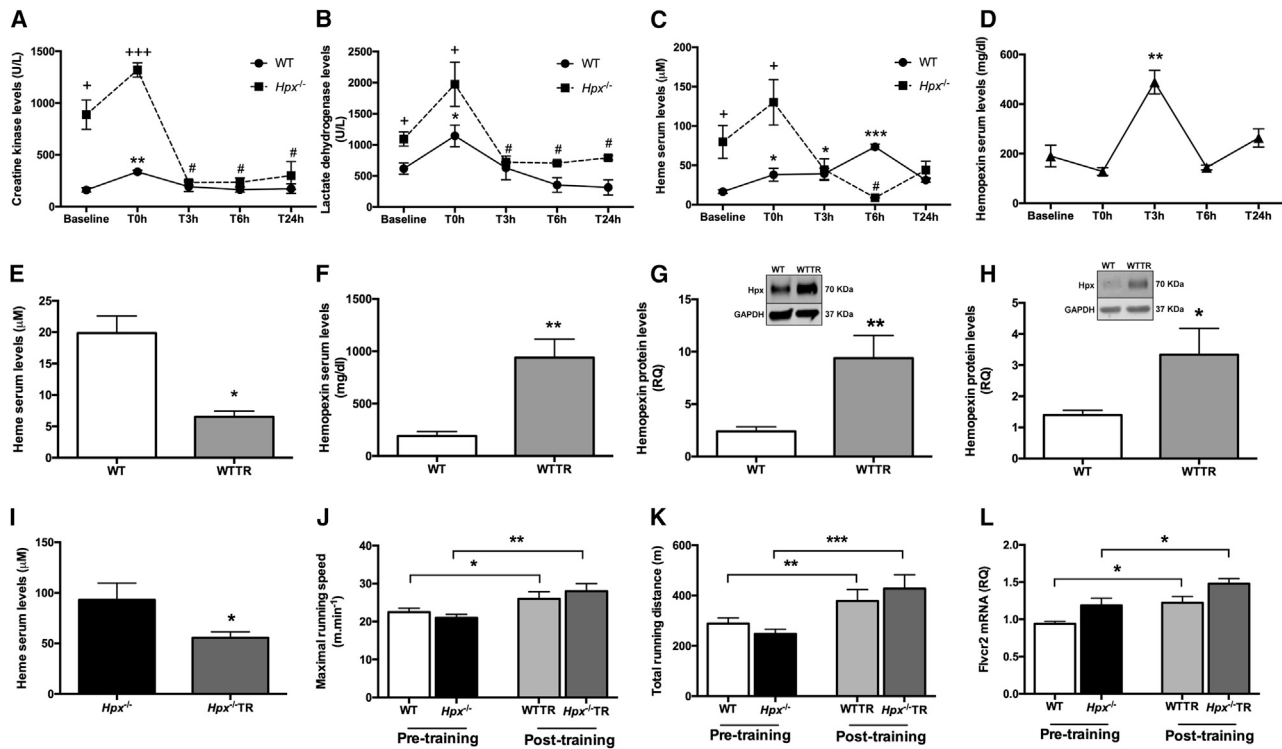


**Figure 2. Aerobic exercise promotes circulating heme release and upregulates hemopexin (Hpx) levels**

(A–D) Serum CK, LDH, heme, and Hpx levels in WT and *Hpx*<sup>-/-</sup> mice at different time points after acute running exercise on a treadmill. Data represent mean ± SEM. \**p* < 0.05, \*\**p* < 0.01, \*\*\**p* < 0.001 versus WT baseline; #*p* < 0.05 versus *Hpx*<sup>-/-</sup> baseline; +*p* < 0.05, +++*p* < 0.001 WT versus *Hpx*<sup>-/-</sup>; *n* = 4–6/time point. (E–H) Serum heme and Hpx levels in the serum, heart, and plantaris muscle after 6 weeks of exercise training in WT (WTTR) mice. (I–K) Serum heme levels in *Hpx*<sup>-/-</sup> mice and running capacity in WT and *Hpx*<sup>-/-</sup> mice before and after 6 weeks of exercise training. (L) *Flvcr2* gene expression in plantaris skeletal muscle before and after 6 weeks of aerobic exercise training in WT and *Hpx*<sup>-/-</sup> mice. Data represent mean ± SEM. \**p* < 0.05, \*\**p* < 0.01, \*\*\**p* < 0.001; *n* = 6/group.

bout, in wild-type (WT) mice, we observed an increase in serum creatine kinase (CK) and lactate dehydrogenase (LDH) as expected, as measures of muscle cell injury (Figures 2A and 2B). In a similar pattern, heme levels begin to increase immediately after the end of exercise, reaching a maximum at 6 h (16.49 ± 2.32 to 73.48 ± 3.46 μM). This increase was aligned with hemopexin levels that peaked 3 h after exercise (Figures 2C and 2D). We hypothesized that the observed elevation in heme-Hpx acutely contributes to tissue recovery and muscle conditioning. To further understand the role of Hpx in acute exercise, we subjected *Hpx*<sup>-/-</sup> mice to the same exercise routine. Although circulating levels of CK, LDH, and heme were significantly elevated over those observed in WT mice basally, their content increased further and then rapidly decreased after exercise, suggesting heme clearance was occurring through alternative mechanisms of action (Figures 2A–2C).

Next, we subjected mice to aerobic exercise training to determine whether there were differences with regard to heme processing occurring over longer periods of conditioning. We subjected WT and *Hpx*<sup>-/-</sup> mice to six weeks of aerobic exercise training (WTTR and *Hpx*<sup>-/-</sup>TR mice, respectively) on a treadmill. In conjunction with an improvement in running capacity, and in contrast to that observed after acute exercise, because exercise training promotes skeletal muscle conditioning and reduces mi-

crotrauma, WTTR mice showed a significant decrease in serum heme levels concomitant with a significant increase in Hpx protein expression in serum, heart, and skeletal muscle (Figures 2E–2H; Figure S1). *Hpx*<sup>-/-</sup> animals subjected to the same exercise training protocol also showed a reduction in circulating heme content in *Hpx*<sup>-/-</sup>TR compared with sedentary *Hpx*<sup>-/-</sup> mice, with no difference in motor coordination before the training protocol or in their running capacity after training (Figures 2I–2K; Figure S2). These findings support Hpx as a critical protein necessary for proper heme regulation but also solidify the contribution of other factors involved in heme clearance, because skeletal muscle adapts to exercise similarly in WT and *Hpx*<sup>-/-</sup> mice. These might include proteins such as haptoglobin (Yusof et al., 2007) and albumin, as well as feline leukemia virus subgroup C receptor 2 (*Flvcr2*), a heme importer that is increased in plantaris skeletal muscle of *Hpx*<sup>-/-</sup> animals after training (Figure 2L). Collectively, these data demonstrate that in the absence of Hpx, a transient elevation in circulating heme after exercise is cleared and results in no difference in exercise capacity, suggesting that overall heme regulation remains undisturbed.

#### Aerobic exercise induces HO-1 expression in mice

Given that heme clearance appeared normal in acute and chronically exercised mice with no effect on running capacity, we next

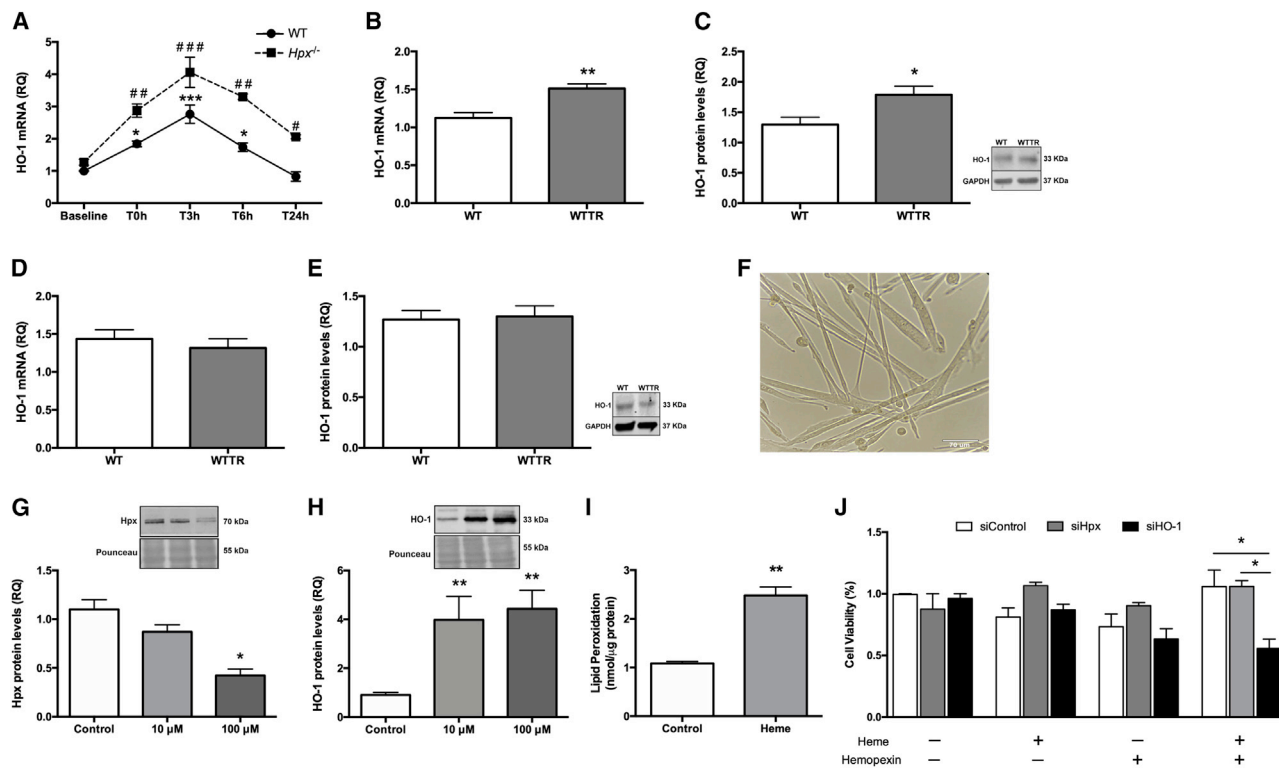


**Figure 3. HO-1 is induced by aerobic exercise**

(A) HO-1 expression in WT and *Hpx*<sup>-/-</sup> mice over time in plantaris muscle after an acute aerobic exercise bout. Data represent mean ± SEM. \**p* < 0.05, \*\*\**p* < 0.001 versus baseline; #*p* < 0.05, ##*p* < 0.01, ###*p* < 0.001 versus *Hpx*<sup>-/-</sup> baseline; *n* = 4–6/time point.

(B–E) HO-1 mRNA and protein expression with representative immunoblots in the plantaris muscle and heart, respectively, after 6 weeks of aerobic exercise training in WT mice. Data represent mean ± SEM. \**p* < 0.05, \*\**p* < 0.01; *n* = 6/group.

(F) Representative image of primary skeletal muscle myotube cells.

(G and H) Hemopexin and HO-1 expression at different concentrations of heme in myotube cells.

(I) Lipid peroxidation levels in myotubes after 4 h of treatment with heme (50 μM).

(J) Myotubes silenced to Hpx (siHpx) and HO-1 (siHO-1) were evaluated for viability after treatment with heme (50 μM) and hemopexin (1 μM).

Data represent mean ± SEM. \**p* < 0.05, \*\**p* < 0.01 versus control.

assessed the role of HO-1, because its activity is critical in regulating inflammation and tissue repair and in catabolizing prooxidant heme (Gozzelino et al., 2010). We observed that WT and *Hpx*<sup>-/-</sup> mice show significantly elevated expression of HO-1 in plantaris muscle 3 h after acute exercise. This increase in expression was reduced in the absence of Hpx (Figure 3A). We also observed modest but significant elevation in HO-1 mRNA expression in WT mice over baseline in soleus muscle at 3 h (1.44 ± 0.11-fold, *p* < 0.05). Likewise, elevation in HO-1 mRNA expression was observed in the hearts of WT mice after acute exercise that was slightly delayed from that in skeletal muscle, which occur at 6 h (1.42 ± 0.08-fold, *p* < 0.05). In addition, we evaluated the effects of chronic aerobic training on HO-1 expression in WT animals and observed a significant increase in HO-1 in skeletal muscle (Figures 3B and 3C), with no change in expression in the heart (Figures 3D and 3E). This was similar to the results observed in the HCR rat.

Our results in both rat and mouse models directed us to next ask whether Hpx and HO-1 upregulation in response to elevated heme observed *in vivo* could be recapitulated *in vitro* in primary skeletal muscle cells. Treatment of differentiated mouse primary

skeletal muscle cells treated with heme showed a dose-dependent decrease in Hpx and a simultaneous increase in HO-1 expression (Figures 3F–3H). Heme treatment increased the amount of lipid peroxidation (Figure 3I), and in cells in which HO-1 expression was blocked with small interfering RNA (siRNA), we observed a >50% decrease in cell viability compared with siControl or Hpx-silenced (siHpx)-transfected cells (Figure 3J; Figure S3). Overall, these data support HO-1 as a central regulator in limiting heme-induced cell damage of skeletal muscle cells, and we posit that it is one mechanism that protects the cell and ultimately affects exercise capacity *in vivo*.

### Absence of HO-1 from skeletal muscle results in atrophy and altered motor performance

To dissect the relationship between exercise and HO-1 in skeletal muscle, we generated a tamoxifen-regulated cre-recombinase driven by the human  $\alpha$ -skeletal actin (HSA-MCM) promoter to selectively delete HO-1 from skeletal muscle. We first characterized these mice (*Tam-HSA-Cre-Hmox1<sup>fl/fl</sup>*), hereafter called MHO-1, and observed a 60%–80% decrease in HO-1

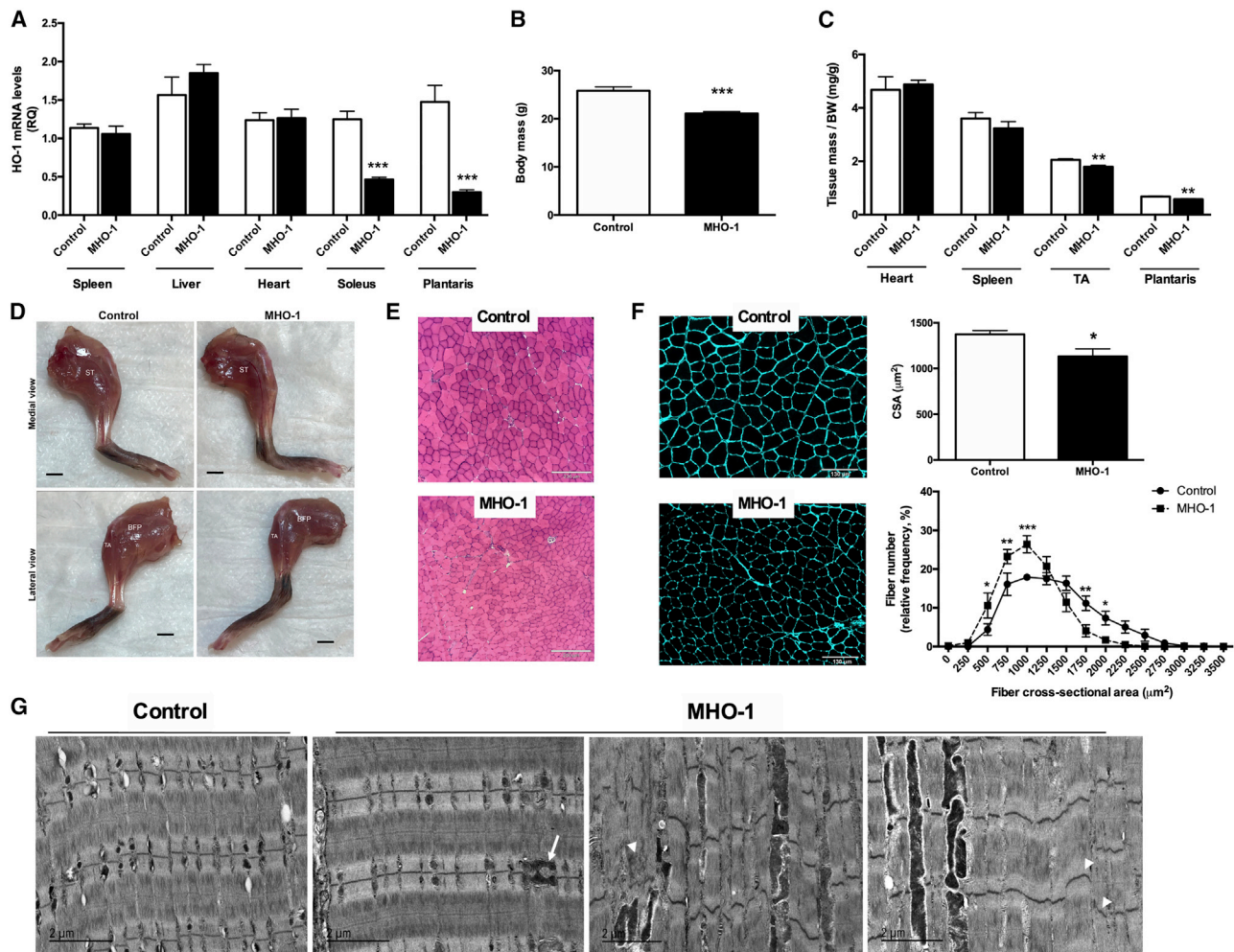


**Figure 4. Absence of HO-1 from skeletal muscle promotes atrophy and altered motor performance**

(A) HO-1 expression in control (*Hmox1<sup>fl/fl</sup>*) and MHO-1 tissues. Expression values were determined by quantitative real-time PCR and normalized to Actb (spleen, liver, and heart) or Hprt1 (soleus and plantaris).

(B and C) Body mass (B) and normalized tissue mass (C) from control and MHO-1 animals. Data represent mean  $\pm$  SEM. \*\* $p < 0.01$ , \*\*\* $p < 0.001$  versus control;  $n = 8$ –10/group.

(D) Representative images of the hindlimb muscles; medial and lateral view, from 10-week-old control and MHO-1 animals. Scale bars: 4 cm.

(E) H&E staining of TA muscles. Note the cross-sectional size differences. Scale bars: 230  $\mu\text{m}$ .

(F) Immunofluorescent staining of tibialis anterior muscles from control and MHO-1 mice stained with anti-laminin (left panel) and quantitative morphometric evaluation of the muscle by mean fiber cross-sectional area (CSA) (right upper panel) and fiber size distribution (right lower panel). Data represent mean  $\pm$  SEM. \* $p < 0.05$ , \*\* $p < 0.01$ , \*\*\* $p < 0.001$  versus control;  $n = 6$ /group. Scale bars: 130  $\mu\text{m}$ .

(G) Electron microscopy (EM) showing muscle ultrastructure of the extensor digitorum longus in control and MHO-1 mice. Control mice exhibited normal myofibrillar architecture, whereas MHO-1 muscles showed areas of enlarged mitochondria (arrow), myofibrillar disorganization, and foci of z disc streaming (arrowhead). Images are representative from 10-week-old male mice ( $n = 3$ /group). Scale bars: 2  $\mu\text{m}$ .

ST, semitendinosus; BFP, biceps femoris (posterior); TA, tibialis anterior.

expression specific to skeletal muscle in mice fed tamoxifen starting from 4–6 weeks of age (Figure 4A). No change in HO-2 expression was observed (Figures S4A and S4B). We also observed no functional or molecular differences in *Hmox1<sup>fl/fl</sup>* control mice fed either regular or tamoxifen chow (Figures S4C–S4F). Because HO-1 is associated with fatty acid synthesis and lipid accumulation (Hinds et al., 2014), we first evaluated muscle anatomy in MHO-1 mice. MHO-1 mice showed a small but significant reduction in whole-body and individual muscle

weights (Figures 4B–4D). To investigate the observed change in muscle mass, we analyzed tibialis anterior (TA) hind-limb muscle, which is similar in composition to plantaris muscle. Assessment of MHO-1 mice revealed normal TA muscle fiber structure but a smaller fiber cross-sectional area (CSA) compared with controls, indicative of atrophy (Figures 4E and 4F). Using extensor longus digitorum muscle from MHO-1 mice, we performed blinded electron microscopic analyses and observed several abnormalities, including intramyocellular lipid droplets,

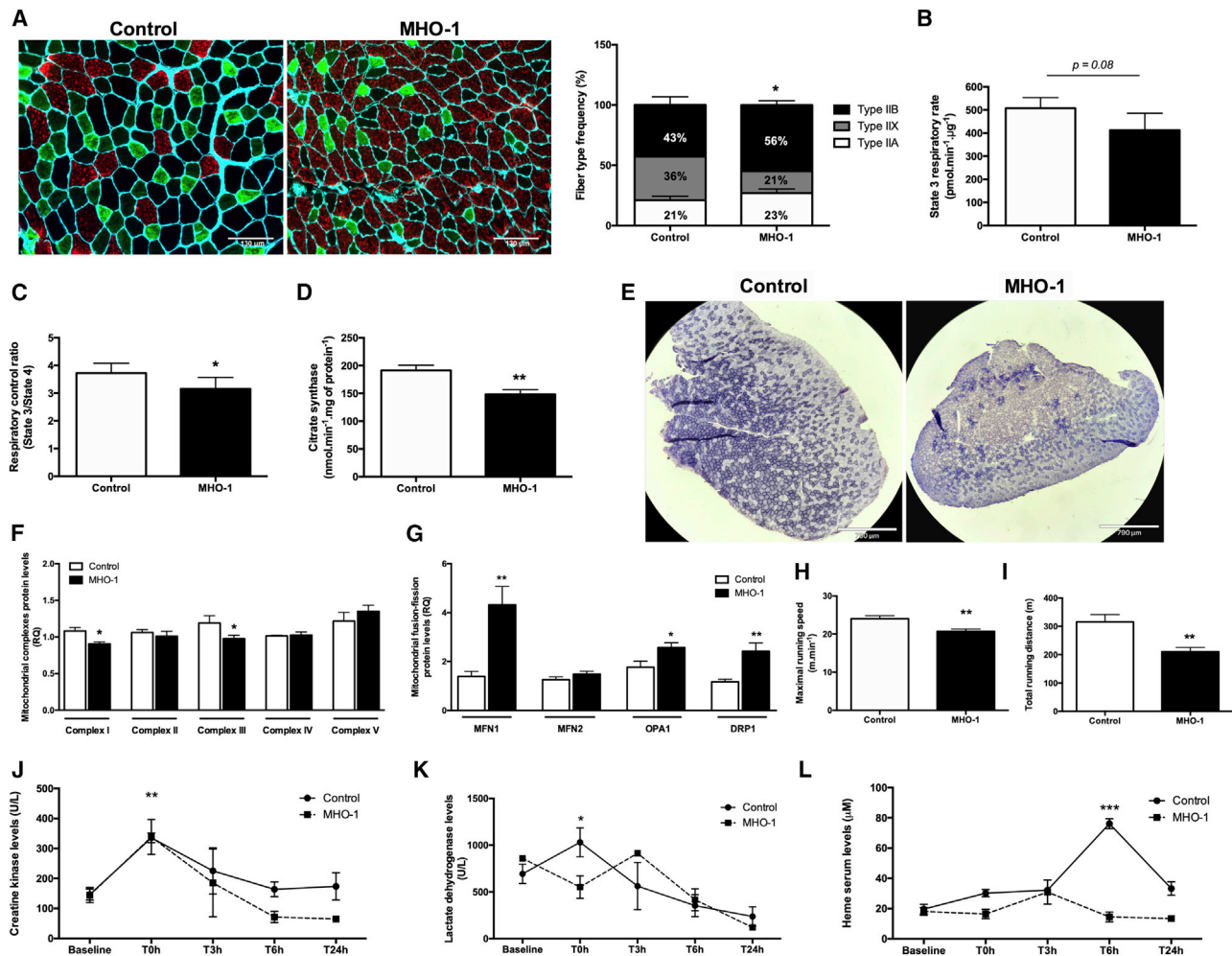


**Figure 5. HO-1-deficient skeletal muscle induces a shift to fast contraction velocity and fatigue susceptibility**

(A) MHO-1 have greater fast-twitch fiber types and decreased running capacity compared with control mice. Representative immunofluorescent staining of tibialis anterior muscle cross-sections for fiber-type identification (left panel) and muscle fiber-type frequency data (right panel). Green, type IIa MyHC isoform; red, type IIb MyHC isoform; black, type IIx MyHC isoform; turquoise, laminin.

(B and C) State 3<sub>ADP</sub> respiratory state (B) and respiratory control ratio (State 3<sub>ADP</sub>/State 4<sub>oligomycin</sub>) (C) in isolated mitochondria from gastrocnemius muscle in the presence of glutamate/malate.

(D and E) Citrate synthase activity (D) and representative images of 10-week-old tibialis anterior muscles stained for succinate dehydrogenase (E).

(F and G) Quantification of mitochondrial complex content and fusion-fission protein expression in plantaris muscle; see also Figure S5.

(H and I) Treadmill maximal running speed and total running distance.

(J–L) Serum CK, LDH, and heme levels at different time points after acute aerobic exercise.

Data represent mean ± SEM. \*p < 0.05, \*\*p < 0.01, \*\*\*p < 0.001 versus baseline; n = 4–6 animals/time point.

enlarged mitochondria, myofibrillar disorganization, and z disc streaming, compared with tissue from control mice (Figure 4G). These data support a role for skeletal muscle HO-1 in fundamental muscle structure and function. In summary, selective deletion of HO-1 from skeletal muscle is linked to changes in body composition and muscle atrophy that partly involve maintaining mitochondrial structure and function.

### Muscle-specific HO-1 deletion promotes fast contraction velocity and fatigue susceptibility

Skeletal muscle is heterogeneous and composed of slow- and fast-twitch fiber types, which differ in the composition of con-

tractile proteins, oxidative capacity, endurance, and fatigability (Baskin et al., 2015). Therefore, we assessed whether HO-1 deletion, specifically in skeletal muscle, was associated with an alteration in muscle fiber transition and fatigue. Fiber composition was altered in the TA muscle of MHO-1 mice compared with control with the proportion of fast-twitch, type IIB fibers significantly increased in TA muscle from MHO-1 animals concomitant with a reduction in type IIX fibers compared with control (Figure 5A). Moreover, type IIB fibers exhibited higher fatigability and lower oxidative capacity, as evidenced by lower mitochondrial enzyme activity (Schiaffino and Reggiani, 1994). To determine the impact of HO-1 on skeletal muscle oxidative capacity,

we next measured mitochondrial respiratory rates in mitochondria isolated from gastrocnemius muscle, comparing MHO-1 with controls. Mitochondria from MHO-1 skeletal muscle displayed lower respiratory rates (respiratory control ratio [RCR] State3/State4) compared with mitochondria from control mice (Figures 5B and 5C). In addition, cells lacking HO-1 showed lower citrate synthase activity and succinate dehydrogenase (SDH) staining intensities, two mitochondrial enzymes involved in oxidative phosphorylation (Figures 5D and 5E). Finally, expression of mitochondrial oxidase complexes I and III were significantly reduced in muscle isolated from MHO-1 mice compared with control (Figure 5F; Figure S5A). Because mitochondrial content is tightly regulated by mitochondrial dynamics (Detmer and Chan, 2007), we next profiled protein expression of the principle guanosine triphosphatases (GTPases) involved in mitochondrial fusion and mitophagy, including mitofusin 1 (MFN1), mitofusin 2 (MFN2), and OPA1 in skeletal muscle. We also measured expression of dynamin-related protein (DRP1), which is involved in mitochondrial fission (Ding et al., 2010). Both large GTPases that mediate mitochondrial fusion and mitophagy (MFN1 and OPA1), as well as fission (DRP1), accumulated in muscle from MHO-1 mice compared with control (Figure 5G; Figure S5B). No change in MFN2 expression was observed. Considering that mitofusin accumulation usually occurs upon proteasomal inactivation, the elevated mitochondrial fusion proteins observed in MHO-1 muscle might reflect impaired proteasomal activity (Tanaka et al., 2010). In addition, the activation of mitochondrial fission machinery may explain muscle wasting observed in MHO-1 mice (Romanello et al., 2010).

The change in muscle morphology and the impairment in mitochondrial health suggested an alteration in motor and exercise performance. To test this, we evaluated motor coordination by rotarod and observed that MHO-1 mice exhibited significantly reduced rotarod times (125.8 s for MHO-1 versus 231.6 s for control,  $p < 0.05$ ). MHO-1 mice also showed significantly lower exercise performance during acute exercise, running nearly 36% less than control mice of equal age (330.3 min for MHO-1 versus 210.5 min for control,  $p < 0.001$ ) (Figures 5H and 5I). Serum CK and LDH levels in MHO-1 mice showed no difference versus controls (Figures 5J and 5K). Intriguingly, heme levels were significantly elevated after acute exercise in controls, as expected, which was not observed in MHO-1 mice (Figure 5L). One explanation may be higher-than-normal hemopexin levels in MHO-1 mice and the likely involvement of other tissue sites capable of clearing and catabolizing heme. These data strongly suggest that HO-1 in skeletal muscle is critical for running capacity and maintaining normal muscle physiology. Collectively, the slow-to-fast conversion observed in muscle from MHO-1 animals was associated with increased susceptibility to fatigue and suggests a cell-specific mechanism by which HO-1 regulates muscle fiber structure, function, and homeostasis in response to exercise.

### Aerobic exercise training worsens skeletal muscle mass in MHO-1 mice

Skeletal muscle abnormalities, such as loss of muscle mass, directly contribute to exercise intolerance and impair daily activities, which makes them strong determinants of quality of life and

overall mortality (Anker et al., 1997). Exercise training represents an intervention that can attenuate or even reverse the process of muscle wasting. Therefore, we next assessed whether HO-1 deletion would interfere with the benefits of aerobic training. Although our aerobic exercise training protocol showed attenuation in running capacity in MHO-1 mice (Figures 6A and 6B), we hypothesized that exercise would prevent muscle wasting in MHO-1 mice compared with control. However, we observed that MHO-1 mice that underwent training (MHO-1-TR) showed decreased body mass, loss of skeletal muscle mass, and decreased muscle weight compared with the control-TR group. Similar differences in mean CSA and distribution were observed when comparing control-TR and MHO-1 animals (Figures 6C–6G). To better understand the correlation between muscle atrophy and HO-1 deletion after training, we next focused on exercise-induced microtrauma and the release of heme. In untrained mice, serum heme was lower in MHO-1 mice versus controls, which corresponded to higher Hpx levels basally (Figures 6H and 6I). After training, MHO-1 mice showed higher serum heme levels and decreased Hpx levels versus those of non-trained controls, in contrast to what we observed in the WT and *Hpx*<sup>-/-</sup> training models (Figures 2E, 2F, 2I, 6H, and 6I). Furthermore, heme levels in plantaris muscles from MHO-1 groups ( $\pm$ TR) were higher versus those from control groups (Figure 6J). These data suggested that excess heme might be functioning as a DAMP in this setting and promoting muscle tissue injury.

Exercise attenuates muscle wasting by targeting both protein synthesis and degradation pathways (Schiaffino et al., 2013). We next investigated whether hypertrophy-related genes were affected by exercise training in the presence and absence of HO-1 in muscle. Although some studies suggest that exercise modulates protein synthesis via activation of the insulin growth factor 1 (IGF-1)-phosphatidylinositol 3-kinase (PI3K)-Akt pathway (Schiaffino and Mammucari, 2011), absence of HO-1 (MHO-1-TR) from muscle inhibited this upregulation with no change in IGF-1 compared with controls (Figure 6K). Considering that satellite cell myogenic regulatory factors (MRFs) also modulate muscle hypertrophy (Blaauw and Reggiani, 2014), we next measured Pax7, MyoD, and myogenin, which are involved in differentiation of satellite cells. Exercise training of MHO-1-TR mice showed a reduction in Pax7 and MyoD transcripts compared with MHO-1 sedentary animals (Figure 6L). Conversely, myogenin, a transcription factor essential for skeletal muscle differentiation (Eftimie et al., 1991; Leikina et al., 2018; Millay et al., 2014), was upregulated in both MHO-1 and MHO-1-TR groups compared with control sedentary animals (Figure 6L). However, two essential muscle-specific myoblast fusion proteins that are induced by myogenin, Myomaker (Mymk), and Myomerger (Mymx), were downregulated in both MHO-1-TR and sedentary animals, suggesting a possible feedback mechanism by which non-fusogenic cells attempt to further differentiate (Figure 6M). When WT animals were exposed to inhaled CO, a bioactive product of HO-1 activity that can induce HO-1 (Lee et al., 2006; Piantadosi et al., 2008), Mymx was upregulated (Figure S6), indicating that HO-1/CO likely contribute to the fusion of muscle cells during development and/or exercise-induced

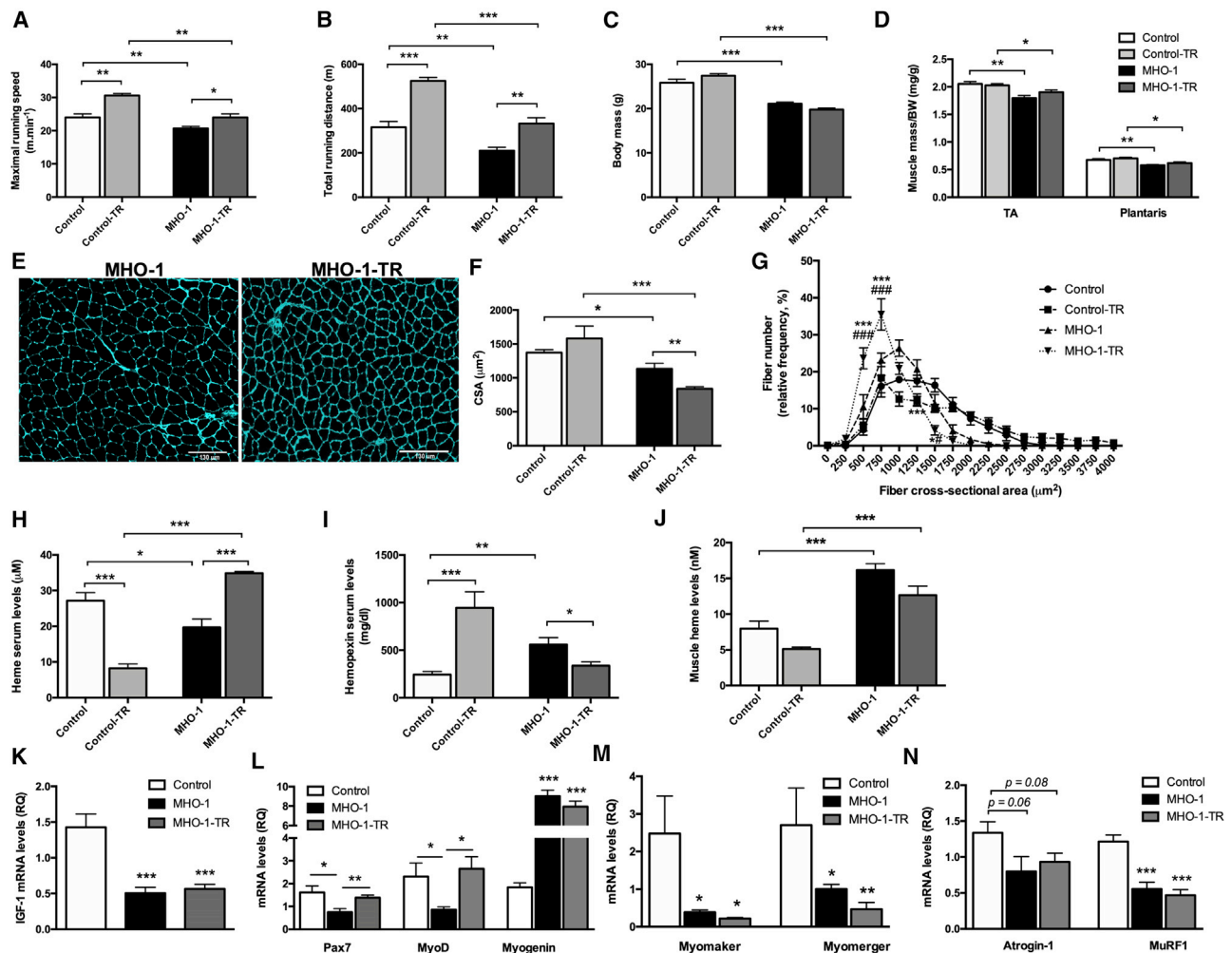


**Figure 6. Aerobic exercise training is harmful to skeletal muscle mass in MHO-1 mice**

(A and B) Maximal treadmill running speed and total running distance in control and MHO-1 submitted or not to 6 weeks of running aerobic training (TR). (C and D) Body mass and normalized muscle mass from control, control-TR, MHO-1, and MHO-1-TR animals. Data represent mean  $\pm$  SEM. \* $p < 0.05$ , \*\* $p < 0.01$ , \*\*\* $p < 0.001$  versus control;  $n = 8$ –10/group. (E–G) Representative immunofluorescent staining images (E) of 10-week-old tibialis anterior muscles from MHO-1 and MHO-1-TR mice stained with an antibody to laminin and morphometric evaluation in sedentary and trained muscle from control and MHO-1 animals by mean fiber CSA (F) and fiber size distribution (G). Data represent mean  $\pm$  SEM. \* $p < 0.05$ , \*\* $p < 0.01$ , \*\*\* $p < 0.001$  versus control-TR; # $p < 0.05$ , ### $p < 0.001$  versus MHO-1;  $n = 8$ –10/group. (H and I) Serum heme and hemopexin levels in control and MHO-1 animals 72 h after the end of aerobic training. (J) Tibialis anterior heme levels in sedentary and trained control and MHO-1 animals. (K–N) mRNA expression in plantaris muscle in control, MHO-1, and MHO-1-TR animals. Data represent mean  $\pm$  SEM. \* $p < 0.05$ , \*\* $p < 0.01$ , \*\*\* $p < 0.001$  versus control;  $n = 6$ .

regeneration. Myogenin has also been associated with muscle atrophy by controlling expression of atrophy-related genes (Moresi et al., 2010). Finally, we investigated two ubiquitin-protein ligases, Atrogin-1 (*Fbxo32*) and MuRF-1 (*Trim63*), both of which were downregulated in muscle from both MHO-1 sedentary and MHO-1-TR groups compared with control (Figure 6N). These ligases are important regulators of muscle mass, and a decrease in their activity is observed with aging. These results, together with the muscle atrophy present in MHO-1 mice, reinforces a role for HO-1 activity in muscle necessary to prevent morphological and metabolic dysfunction caused by exercise training. These data strongly

support the concept that heme metabolism is critically involved in muscle conditioning.

## DISCUSSION

Given the association between high aerobic capacity and prevention of metabolic diseases (Booth et al., 2012), elucidating the mechanisms by which high aerobic capacity regulates whole-body metabolic homeostasis is still a major research challenge. The heme-Hpx-HO-1 axis is a well-recognized acute phase mechanism that is activated during disease and pathophysiological conditions, such as sepsis and trauma (Barreiro

et al., 2002; Chiabrando et al., 2014; Graw et al., 2016). In contrast, the regulation, function, and importance of this signaling pathway in situations favorable to health, such as physical exercise, remain unknown. Here, we delineate an essential role for heme metabolism focused on HO-1 and provide data supporting its role in maintenance of skeletal muscle morphology and function using gain- and loss-of-function approaches *in vitro* and *in vivo*.

Heme plays an essential role in numerous biological processes in aerobic organisms, which range from reversible oxygen binding to electron transport of the respiratory chain (Hamza and Dailey, 2012; Wagener et al., 2003). However, despite its well-established physiological functions, heme can be harmful as a DAMP and critically involved in the pathogenesis of various disease pathologies, such as trauma, sickle cell disease, infection, and sterile inflammation. Each of them results in the release of large amounts of hemoproteins into the circulation (Reeder, 2010; Schaer et al., 2014). Physical exercise has also been linked with hemolysis, although by different proposed mechanisms, including mechanical damage to red blood cells as they pass through capillaries (Telford et al., 2003), continuous exposure to high-oxygen flux (Smith, 1995), and perturbation of osmotic homeostasis (Green et al., 1991). Moreover, exercise induces skeletal muscle microtrauma, a phenomenon commonly known as exercise-induced muscle damage, and is characterized by loss of muscle cell integrity and a sterile inflammatory response (Deli et al., 2017; Fehrenbach and Schneider, 2006; Margonis et al., 2007). Considering that both mechanisms are responsible for extracellular heme release, we demonstrate here that acute aerobic exercise promotes a time-dependent release of heme into the circulation. In addition, or in conjunction with direct effects on the cell, heme acts indirectly via induction of HO-1 toward the generation of cytoprotective and bioactive heme degradation products, including carbon monoxide and bile pigments (Otterbein et al., 2003). In contrast, wild-type animals subjected to aerobic training for six weeks or animals with an intrinsically higher aerobic capacity (HCR), we observed a decrease in serum heme levels. This is likely dictated partly by a protective phenotype that develops in skeletal muscle following exercise training (exercise preconditioning), in conjunction with more efficient heme clearance. Altogether, these observations suggest that upregulation of other acute phase proteins during exercise training, such as Hpx, haptoglobin, and Flvcr2, can bind and transport heme to be metabolized by HO-1 intracellularly (Alonso et al., 2018; Schaer et al., 2014). For instance, in the absence of HO-1, but not Hpx, heme is highly toxic and increases lipid peroxidation and cell death in primary skeletal muscle cells, suggesting metabolism versus binding is an important determinant. Thus, these specific cellular events regulate metabolic and energetic pathways to ensure cell and tissue survival and, in the context of skeletal muscle, adaptation and capacity.

Hemopexin is found in humans and animals with higher aerobic capacities (Kohler et al., 2010; Souza et al., 2018). The primary function of Hpx appears to be neutralization and scavenging of excess free heme from the circulation (Vinchi et al., 2013). In our study, HCR animals presented elevated Hpx levels compared with LCR animals. Moreover, not just a higher intrinsic

aerobic capacity observed in HCR but also improved aerobic capacity with exercise training upregulated Hpx expression in serum, heart, and skeletal muscle of WT animals and may indicate a hemolytic process that occurs during repetitive running sessions (Kohler et al., 2010). Remarkably, even Hpx-deficient animals, in which we observed significantly elevated CK, LDH, and heme levels in comparison to WT control mice, both basally and immediately after exercise, had a rapid decrease in their circulating levels and no difference in running capacity before or after exercise training.

As a stress-inducible enzyme, HO-1 plays a critical role in protecting cells from oxidative stress (Kumar and Bandyopadhyay, 2005), and removal of heme to prevent free radical formation is critical. The products of HO-1 activity, including carbon monoxide and bilirubin, are responsible for the benefits ascribed to HO-1. Primary skeletal muscle cells missing HO-1 are highly susceptible to apoptosis and cell death (Kozakowska et al., 2012). However, HO-1 activation by heme attenuates skeletal muscle atrophy induced by immobilization (Park et al., 2013). Upregulation of HO-1 can protect against exercise-induced injury in both human and rat skeletal muscle (Ghio et al., 2018; Pilegaard et al., 2000). Absence of HO-1 specifically from skeletal muscle (MHO-1) was highly damaging to muscle tissue. Therefore, HO-1 must be considered a central mediator responsible for modulating the intensity of muscle injury and function. Moreover, the cumulative effects of transient increases in HO-1 during exercise recovery represent a mechanism by which the cell and tissue respond and adapt to exercise.

HO-1-deficient myofibers showed skeletal muscle abnormalities, including changes in morphology, function, and depressed skeletal muscle aerobic capacity. These alterations were associated with the presence of z disc streaming and lipid droplet accumulation compared with normal muscle fibers (Grobler et al., 2004). These morphological abnormalities and accumulation of glycogen and lipid droplets in skeletal muscle from MHO-1 mice may indicate muscle damage, non-specific muscle pathology, or mitochondrial deficiency. Lack of HO-1 correlated with a decrease in oxidative metabolism—evidenced by lower SDH staining, lower citrate synthase activity, and disruption in mitochondrial quality control, which is characterized by increased mitochondrial fragmentation and reduced function—has been reported to occur in muscle during chronic disease, such as cancer and heart failure (Yoshida and Delafontaine, 2015). This generalized myopathy is characterized by a shift from an oxidative to a more glycolytic phenotype in skeletal muscle mitochondria (Bacurau et al., 2016). Collectively, these observed metabolic alterations support a role for HO-1 in regulating fiber composition and muscle fiber CSA of glycolytic muscle. In addition, HO-1 cooperates with other factors related to fiber muscle transition and/or mass, such as satellite cell MRFs (Pax7, MyoD, and myogenin) and IGF-1, respectively, toward maintaining muscle mass and function (Schiaffino et al., 2013). We find that Pax7 and MyoD genes, as markers of quiescent and proliferating satellite cells, and IGF-1 were reduced in the absence of HO-1 (Glass, 2003). HO-1 is a potent regulator of proliferation and differentiation of satellite cells into myocytes and myotubes (Kozakowska et al., 2012). In C2C12 murine

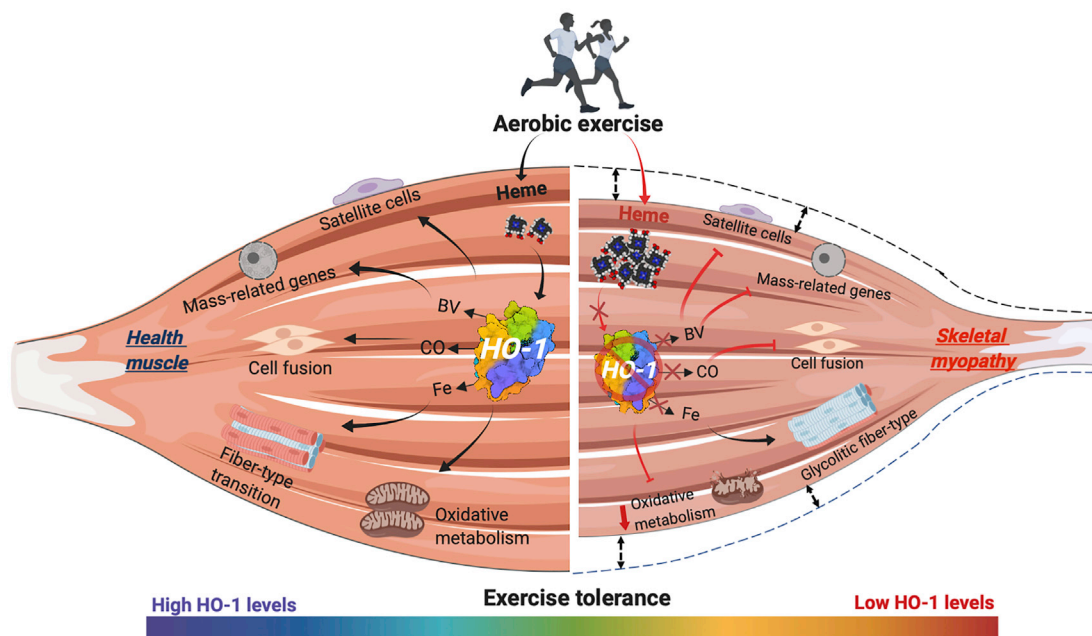


**Figure 7. Proposed model for how skeletal muscle HO-1 activity regulates aerobic capacity and muscle performance**

Skeletal muscle microtraumas occur during aerobic exercise and result in elevated heme levels, inducing the expression of HO-1. Aerobic exercise training increases HO-1, which enhances muscle function by modulating satellite cell activation/proliferation, myoblast fusion, hypertrophy/atrophy-related genes, fiber-type transition, and mitochondrial function (left panel). Exercise training, which counteracts skeletal myopathy, was unable to function appropriately in the absence of HO-1 (right side). We propose that the accumulation of intracellular heme results in muscle myopathy, as evidenced by atrophy and exercise intolerance. This illustration was created using icons from BioRender (<https://biorender.com/>) and Servier Medical Art (<https://smart.servier.com/>).

myoblasts or primary mouse myoblasts, inhibition or overexpression of HO-1 during muscle cell differentiation changed the myogenic program in which HO-1 upregulation increased proliferation of myoblasts, whereas differentiation into myotubes was strongly reduced. Similarly, myogenin, a transcription factor essential for skeletal muscle differentiation and associated with muscle atrophy (Moresi et al., 2010), was significantly upregulated in MHO-1 mice versus controls. We posit that myogenin upregulation could be a compensatory feedback mechanism by which non-fusogenic cells attempt to further differentiate. Regarding muscle cell fusion, Myrk and Mymx, two essential muscle-specific membrane proteins that control myoblast fusion (Leikina et al., 2018; Millay et al., 2014) were reduced in HO-1-deficient skeletal muscle. Moreover, CO exposure, as a bioactive product of HO-1 activity (Lee et al., 2006; Otterbein et al., 2016; Piantadosi et al., 2008), significantly increased Mymx mRNA in plantaris skeletal muscle (Figure S6). Based on these proteins dividing their fusogenic activities to initiate and drive membrane coalescence and muscle formation, we posit that elevated intracellular heme in muscle from MHO-1 animals may promote destabilization and reduce lipid membrane proteins. Furthermore, HO-1 is necessary to ensure fusion of proper muscle cells during development and/or regeneration.

Considering that aerobic exercise training is a powerful tool counteracting skeletal myopathy, we expected that exercising would prevent muscle wasting in MHO-1 mice (Booth et al., 2012; Brum et al., 2011; Gabriel and Zierath, 2017). We observed

that exercise training worsened muscle morphology and function in MHO-1 mice compared with controls, perhaps because HO-1 deficiency results in persistent skeletal muscle injury during exercise training. Our data have identified a role for HO-1 in muscle remodeling and the impact on muscle damage and repair responses. Mechanistically, myogenin has been shown to regulate expression of the E3 ubiquitin ligases MuRF1 and atrogin-1, promoting muscle proteolysis and atrophy. MHO-1 and MHO-1-TR animals did not show increased expression of these atrophy-related genes, which are typically increased as muscles atrophy (Edström et al., 2006; Sartorelli and Fulco, 2004). Moreover, sarcopenic skeletal muscle is a major age-related phenotype that includes mitochondrial dysfunction and requires prolonged regenerative activity (Edström et al., 2006; Su et al., 2015). Thus, our working model is that the lack of HO-1 in a sarcopenic-like muscle impairs and delays recovery after exercise training (Figure 7).

In summary, these data delineate a facet of heme biology and exercise physiology supported by studies in animals lacking hemoxygenin and HO-1, two proteins involved in the transport and metabolism of heme. We find that although heme is elevated, the inability of heme metabolism to occur specifically in skeletal muscle results in mitochondrial dysfunction, skeletal muscle atrophy, and a profound inability to adapt to exercise metabolically compared with littermate controls. Altogether, these data provide critical information related to heme biology and its role in skeletal muscle and may prove useful in furthering our understanding of the physiology of aerobic exercise, adaptation, and conditioning.

## STAR★METHODS

Detailed methods are provided in the online version of this paper and include the following:

- **KEY RESOURCES TABLE**
- **RESOURCE AVAILABILITY**
  - Lead contact
  - Materials availability
  - Data and code availability
- **EXPERIMENTAL MODEL AND SUBJECT DETAILS**
- **METHOD DETAILS**
  - Graded treadmill exercise test and aerobic exercise protocols
  - Rotarod performance
  - Mitochondrial isolation and activity
  - Heme and hemopexin content
  - Biochemical analyses
  - Quantitative real-time PCR
  - Immunoblotting
  - Cell culture
  - Analysis of skeletal muscle damage
  - Histological analysis
  - Transmission electron microscopy
- **QUANTIFICATION AND STATISTICAL ANALYSIS**

## SUPPLEMENTAL INFORMATION

Supplemental information can be found online at <https://doi.org/10.1016/j.celrep.2021.109018>.

## ACKNOWLEDGMENTS

This research was supported by grants from the Department of Defense (W81XWH-16-0464); NIH (R43GM125430); the National Football League Players Association; and (R01DK119202 to L.E.O.); the São Paulo Research Foundation (FAPESP), Brazil (2015/228145 to P.C.B. and 14/25957-9 and 17/19954-5 to R.W.A.d.S.); the National Council for Scientific and Technological Development (CNPq), Brazil (306261/2016-2 to P.C.B.); and the American Heart Association (19CDA34760244 to R.W.A.d.S.). We thank Susan J. Hagen and the Electron Microscopy core at BIDMC (NIH S10 OD019988). The LCR-HCR rat model system was supported by the Office of Research Infrastructure Programs (OD grant ROD012098A to L.G.K. and S.L.B.) from the NIH.

## AUTHOR CONTRIBUTIONS

R.W.A.d.S., P.C.B., and L.E.O. conceived and designed the study; R.W.A.d.S., A.S., J.W., D.G., L.G.K., S.L.B., and U.W. carried out the animal procedures and *in vivo* experiments; R.W.A.d.S. performed laboratorial experiments and G.R.L., A.S., E.K., G.C.T., and E.C. contributed to them; R.W.A.d.S. and E.K. analyzed the data; and R.W.A.d.S. and L.E.O. wrote the manuscript.

## DECLARATION OF INTERESTS

L.E.O. is a scientific advisor for Hillhurst Biopharmaceuticals. The remaining authors declare no competing interests.

Received: July 20, 2020

Revised: March 8, 2021

Accepted: March 30, 2021

Published: April 20, 2021

## REFERENCES

- Alonso, I., Matos, A., Ribeiro, R., Gil, Á., Cardoso, C., Sardinha, L.B., and Bicho, M. (2018). Mountain Cycling Ultramarathon Effects on Inflammatory and Hemoglobin Responses. *Med. Sci. Sports Exerc.* *50*, 353–360.
- Anker, S.D., Ponikowski, P., Varney, S., Chua, T.P., Clark, A.L., Webb-Peploe, K.M., Harrington, D., Kox, W.J., Poole-Wilson, P.A., and Coats, A.J. (1997). Wasting as independent risk factor for mortality in chronic heart failure. *Lancet* *349*, 1050–1053.
- Bacurau, A.V., Cunha, T.F., Souza, R.W., Voltarelli, V.A., Gabriel-Costa, D., and Brum, P.C. (2016). Aerobic Exercise and Pharmacological Therapies for Skeletal Myopathy in Heart Failure: Similarities and Differences. *Oxid. Med. Cell. Longev.* *2016*, 4374671.
- Barreiro, E., Comtois, A.S., Mohammed, S., Lands, L.C., and Hussain, S.N. (2002). Role of heme oxygenases in sepsis-induced diaphragmatic contractile dysfunction and oxidative stress. *Am. J. Physiol. Lung Cell. Mol. Physiol.* *283*, L476–L484.
- Baskin, K.K., Winders, B.R., and Olson, E.N. (2015). Muscle as a “mediator” of systemic metabolism. *Cell Metab.* *21*, 237–248.
- Blaauw, B., and Reggiani, C. (2014). The role of satellite cells in muscle hypertrophy. *J. Muscle Res. Cell Motil.* *35*, 3–10.
- Blanco, C.E., Sieck, G.C., and Edgerton, V.R. (1988). Quantitative histochemical determination of succinic dehydrogenase activity in skeletal muscle fibres. *Histochem. J.* *20*, 230–243.
- Booth, F.W., Roberts, C.K., and Laye, M.J. (2012). Lack of exercise is a major cause of chronic diseases. *Compr. Physiol.* *2*, 1143–1211.
- Brum, P.C., Bacurau, A.V.N., Medeiros, A., Ferreira, J.C.B., Vanzelli, A.S., and Negrão, C.E. (2011). Aerobic exercise training in heart failure: impact on sympathetic hyperactivity and cardiac and skeletal muscle function. *Braz. J. Med. Biol. Res.* *44*, 827–835.
- Chan, M.C., Ziegler, O., Liu, L., Rowe, G.C., Das, S., Otterbein, L.E., and Arany, Z. (2016). Heme oxygenase and carbon monoxide protect from muscle dystrophy. *Skelet. Muscle* *6*, 41.
- Chiabrando, D., Vinchi, F., Fiorito, V., Mercurio, S., and Tolosano, E. (2014). Heme in pathophysiology: a matter of scavenging, metabolism and trafficking across cell membranes. *Front. Pharmacol.* *5*, 61.
- DeLi, C.K., Fatouros, I.G., Paschalis, V., Tsiokanos, A., Georgakouli, K., Zalavras, A., Avloniti, A., Koutedakis, Y., and Jamurtas, A.Z. (2017). Iron Supplementation Effects on Redox Status following Aseptic Skeletal Muscle Trauma in Adults and Children. *Oxid. Med. Cell. Longev.* *2017*, 4120421.
- Detmer, S.A., and Chan, D.C. (2007). Functions and dysfunctions of mitochondrial dynamics. *Nat. Rev. Mol. Cell Biol.* *8*, 870–879.
- Ding, H., Jiang, N., Liu, H., Liu, X., Liu, D., Zhao, F., Wen, L., Liu, S., Ji, L.L., and Zhang, Y. (2010). Response of mitochondrial fusion and fission protein gene expression to exercise in rat skeletal muscle. *Biochim. Biophys. Acta* *1800*, 250–256.
- Edström, E., Altun, M., Hägglund, M., and Ulfhake, B. (2006). Atrogin-1/MAFbx and MuRF1 are downregulated in aging-related loss of skeletal muscle. *J. Gerontol. A Biol. Sci. Med. Sci.* *61*, 663–674.
- Eftimie, R., Brenner, H.R., and Buonanno, A. (1991). Myogenin and MyoD join a family of skeletal muscle genes regulated by electrical activity. *Proc. Natl. Acad. Sci. USA* *88*, 1349–1353.
- Fehrenbach, E., and Schneider, M.E. (2006). Trauma-induced systemic inflammatory response versus exercise-induced immunomodulatory effects. *Sports Med.* *36*, 373–384.
- Ferreira, J.C.B., Rolim, N.P.L., Bartholomeu, J.B., Gobatto, C.A., Kokubun, E., and Brum, P.C. (2007). Maximal lactate steady state in running mice: effect of exercise training. *Clin. Exp. Pharmacol. Physiol.* *34*, 760–765.
- Gabriel, B.M., and Zierath, J.R. (2017). The Limits of Exercise Physiology: From Performance to Health. *Cell Metab.* *25*, 1000–1011.
- Ghio, A.J., Case, M.W., and Soukup, J.M. (2018). Heme oxygenase activity increases after exercise in healthy volunteers. *Free Radic. Res.* *52*, 267–272.

- Gilligan, D.R., Altschule, M.D., and Katersky, E.M. (1943). Physiological intravascular hemolysis of exercise. Hemoglobinemia and hemoglobinuria following cross-country runs. *J. Clin. Invest.* **22**, 859–869.
- Glass, D.J. (2003). Molecular mechanisms modulating muscle mass. *Trends Mol. Med.* **9**, 344–350.
- Gozzelino, R., Jeney, V., and Soares, M.P. (2010). Mechanisms of cell protection by heme oxygenase-1. *Annu. Rev. Pharmacol. Toxicol.* **50**, 323–354.
- Graw, J.A., Mayeur, C., Rosales, I., Liu, Y., Sabbisetti, V.S., Riley, F.E., Rechechter, O., Malhotra, R., Warren, H.S., Colvin, R.B., et al. (2016). Haptoglobin or hemopexin therapy prevents acute adverse effects of resuscitation after prolonged storage of red cells. *Circulation* **134**, 945–960.
- Green, H.J., Sutton, J.R., Coates, G., Ali, M., and Jones, S. (1991). Response of red cell and plasma volume to prolonged training in humans. *J Appl Physiol* (1985) **70**, 1810–1815.
- Grobler, L.A., Collins, M., Lambert, M.I., Sinclair-Smith, C., Derman, W., St Clair Gibson, A., and Noakes, T.D. (2004). Skeletal muscle pathology in endurance athletes with acquired training intolerance. *Br. J. Sports Med.* **38**, 697–703.
- Hamza, I., and Dailey, H.A. (2012). One ring to rule them all: trafficking of heme and heme synthesis intermediates in the metazoans. *Biochim. Biophys. Acta* **1823**, 1617–1632.
- Hinds, T.D., Jr., Sodhi, K., Meadows, C., Fedorova, L., Puri, N., Kim, D.H., Peterson, S.J., Shapiro, J., Abraham, N.G., and Kappas, A. (2014). Increased HO-1 levels ameliorate fatty liver development through a reduction of heme and recruitment of FGF21. *Obesity (Silver Spring)* **22**, 705–712.
- Hvidberg, V., Maniecki, M.B., Jacobsen, C., Højrup, P., Møller, H.J., and Moestrup, S.K. (2005). Identification of the receptor scavenging hemopexin-heme complexes. *Blood* **106**, 2572–2579.
- Immenschuh, S., Vijayan, V., Janciauskiene, S., and Gueler, F. (2017). Heme as a Target for Therapeutic Interventions. *Front. Pharmacol.* **8**, 146.
- Koch, L.G., and Britton, S.L. (2001). Artificial selection for intrinsic aerobic endurance running capacity in rats. *Physiol. Genomics* **5**, 45–52.
- Kohler, M., Walpurgis, K., Thomas, A., de Maree, M., Mester, J., Schänzer, W., and Thevis, M. (2010). Effects of endurance exercise on the urinary proteome analyzed by 2-D PAGE and Orbitrap MS. *Proteomics Clin. Appl.* **4**, 568–576.
- Kokkinos, P., Myers, J., Kokkinos, J.P., Pittaras, A., Narayan, P., Manolis, A., Karasik, P., Greenberg, M., Papademetriou, V., and Singh, S. (2008). Exercise capacity and mortality in black and white men. *Circulation* **117**, 614–622.
- Kozakowska, M., Ciesla, M., Stefanska, A., Skrzypek, K., Was, H., Jazwa, A., Grochot-Przeczek, A., Kotlinowski, J., Szymula, A., Bartelik, A., et al. (2012). Heme oxygenase-1 inhibits myoblast differentiation by targeting myomirs. *Antioxid. Redox Signal.* **16**, 113–127.
- Kumar, S., and Bandyopadhyay, U. (2005). Free heme toxicity and its detoxification systems in human. *Toxicol. Lett.* **157**, 175–188.
- Lee, B.S., Heo, J., Kim, Y.M., Shim, S.M., Pae, H.O., Kim, Y.M., and Chung, H.T. (2006). Carbon monoxide mediates heme oxygenase 1 induction via Nrf2 activation in hepatoma cells. *Biochem. Biophys. Res. Commun.* **343**, 965–972.
- Leikina, E., Gamage, D.G., Prasad, V., Goykhberg, J., Crowe, M., Diao, J., Kozlov, M.M., Chernomordik, L.V., and Millay, D.P. (2018). Myomaker and Myomergin Work Independently to Control Distinct Steps of Membrane Remodeling during Myoblast Fusion. *Dev. Cell* **46**, 767–780.e7.
- Margonis, K., Fatouros, I.G., Jamurtas, A.Z., Nikolaidis, M.G., Douroudos, I., Chatzinikolaou, A., Mitrakou, A., Mastorakos, G., Papassotiropoulos, I., Taxildaris, K., and Kouretas, D. (2007). Oxidative stress biomarkers responses to physical overtraining: implications for diagnosis. *Free Radic. Biol. Med.* **43**, 901–910.
- Megeney, L.A., Perry, R.L.S., LeCouter, J.E., and Rudnicki, M.A. (1996). bFGF and LIF signaling activates STAT3 in proliferating myoblasts. *Dev. Genet.* **19**, 139–145.
- Millay, D.P., Sutherland, L.B., Bassel-Duby, R., and Olson, E.N. (2014). Myomaker is essential for muscle regeneration. *Genes Dev.* **28**, 1641–1646.
- Moresi, V., Williams, A.H., Meadows, E., Flynn, J.M., Potthoff, M.J., McAnally, J., Shelton, J.M., Backs, J., Klein, W.H., Richardson, J.A., et al. (2010). Myogenin and class II HDACs control neurogenic muscle atrophy by inducing E3 ubiquitin ligases. *Cell* **143**, 35–45.
- Neya, S. (2013). Dynamic motion and rearranged molecular shape of heme in myoglobin: structural and functional consequences. *Molecules* **18**, 3168–3182.
- Otterbein, L.E., Soares, M.P., Yamashita, K., and Bach, F.H. (2003). Heme oxygenase-1: unleashing the protective properties of heme. *Trends Immunol.* **24**, 449–455.
- Otterbein, L.E., Foresti, R., and Motterlini, R. (2016). Heme Oxygenase-1 and Carbon Monoxide in the Heart: The Balancing Act Between Danger Signaling and Pro-Survival. *Circ. Res.* **118**, 1940–1959.
- Park, C.H., Ju, T.J., Kim, Y.W., Dan, J.M., Kim, J.Y., Kim, Y.D., Seo, J.S., and Park, S.Y. (2013). Hemin, heme oxygenase-1 inducer, attenuates immobilization-induced skeletal muscle atrophy in mice. *Life Sci.* **92**, 740–746.
- Piantadosi, C.A., Carraway, M.S., Babiker, A., and Suliman, H.B. (2008). Heme oxygenase-1 regulates cardiac mitochondrial biogenesis via Nrf2-mediated transcriptional control of nuclear respiratory factor-1. *Circ. Res.* **103**, 1232–1240.
- Pilegaard, H., Ordway, G.A., Saltin, B., and Neufer, P.D. (2000). Transcriptional regulation of gene expression in human skeletal muscle during recovery from exercise. *Am. J. Physiol. Endocrinol. Metab.* **279**, E806–E814.
- Reeder, B.J. (2010). The redox activity of hemoglobins: from physiologic functions to pathologic mechanisms. *Antioxid. Redox Signal.* **13**, 1087–1123.
- Ren, C., Qi, J., Li, W., and Zhang, J. (2016). The effect of moderate-intensity exercise on the expression of HO-1 mRNA and activity of HO in cardiac and vascular smooth muscle of spontaneously hypertensive rats. *Can. J. Physiol. Pharmacol.* **94**, 448–454.
- Romanello, V., Guadagnin, E., Gomes, L., Roder, I., Sandri, C., Petersen, Y., Milan, G., Masiero, E., Del Piccolo, P., Foretz, M., et al. (2010). Mitochondrial fission and remodelling contributes to muscle atrophy. *EMBO J.* **29**, 1774–1785.
- Sartorelli, V., and Fulco, M. (2004). Molecular and cellular determinants of skeletal muscle atrophy and hypertrophy. *Sci. STKE* **2004**, re11.
- Schaer, D.J., Vinchi, F., Ingoglia, G., Tolosano, E., and Buehler, P.W. (2014). Haptoglobin, hemopexin, and related defense pathways—basic science, clinical perspectives, and drug development. *Front. Physiol.* **5**, 415.
- Schiaffino, S., and Mammucari, C. (2011). Regulation of skeletal muscle growth by the IGF1-Akt/PKB pathway: insights from genetic models. *Skelet. Muscle* **1**, 4.
- Schiaffino, S., and Reggiani, C. (1994). Myosin isoforms in mammalian skeletal muscle. *J. Appl. Physiol.* **77**, 493–501.
- Schiaffino, S., Dyar, K.A., Ciciliot, S., Blaauw, B., and Sandri, M. (2013). Mechanisms regulating skeletal muscle growth and atrophy. *FEBS J.* **280**, 4294–4314.
- Schneider, Caroline, A., Rasband, Wayne, S., and Eliceiri, Kevin, W. (2012). NIH Image to ImageJ: 25 years of image analysis. *Nature Methods* **9**, 671–675. <https://doi.org/10.1038/nmeth.2089>.
- Smith, J.A. (1995). Exercise, training and red blood cell turnover. *Sports Med.* **19**, 9–31.
- Smith, L.R., and Barton, E.R. (2014). SMASH—semi-automatic muscle analysis using segmentation of histology: a MATLAB application. *Skelet. Muscle* **4**, 21.
- Souza, R.W.A., Alves, C.R.R., Medeiros, A., Rolim, N., Silva, G.J.J., Moreira, J.B.N., Alves, M.N., Wohlwend, M., Gebriel, M., Hagen, L., et al. (2018). Differential regulation of cysteine oxidative post-translational modifications in high and low aerobic capacity. *Sci. Rep.* **8**, 17772.
- Su, J., Ekman, C., Oskolkov, N., Lahti, L., Ström, K., Brazma, A., Groop, L., Rung, J., and Hansson, O. (2015). A novel atlas of gene expression in human skeletal muscle reveals molecular changes associated with aging. *Skelet. Muscle* **5**, 35.

Tanaka, A., Cleland, M.M., Xu, S., Narendra, D.P., Suen, D.F., Karbowski, M., and Youle, R.J. (2010). Proteasome and p97 mediate mitophagy and degradation of mitofusins induced by Parkin. *J. Cell Biol.* *191*, 1367–1380.

Telford, R.D., Sly, G.J., Hahn, A.G., Cunningham, R.B., Bryant, C., and Smith, J.A. (2003). Footstrike is the major cause of hemolysis during running. *J. Appl. Physiol.* *94*, 38–42.

Tolosano, E., and Altruda, F. (2002). Hemopexin: structure, function, and regulation. *DNA Cell Biol.* *21*, 297–306.

Vinchi, F., De Franceschi, L., Ghigo, A., Townes, T., Cimino, J., Silengo, L., Hirsch, E., Altruda, F., and Tolosano, E. (2013). Hemopexin therapy improves cardiovascular function by preventing heme-induced endothelial toxicity in mouse models of hemolytic diseases. *Circulation* *127*, 1317–1329.

Wagener, F.A.D.T.G., Volk, H.D., Willis, D., Abraham, N.G., Soares, M.P., Adema, G.J., and Figdor, C.G. (2003). Different faces of the heme-heme oxygenase system in inflammation. *Pharmacol. Rev.* *55*, 551–571.

Wisloff, U., Najjar, S.M., Ellingsen, O., Haram, P.M., Swoap, S., Al-Share, Q., Fernström, M., Rezaei, K., Lee, S.J., Koch, L.G., and Britton, S.L. (2005). Cardiovascular risk factors emerge after artificial selection for low aerobic capacity. *Science* *307*, 418–420.

Yoshida, T., and Delafontaine, P. (2015). Mechanisms of cachexia in chronic disease states. *Am. J. Med. Sci.* *350*, 250–256.

Yusof, A., Leithauser, R.M., Roth, H.J., Finkernagel, H., Wilson, M.T., and Benke, R. (2007). Exercise-induced hemolysis is caused by protein modification and most evident during the early phase of an ultraendurance race. *J. Appl. Physiol.* *102*, 582–586.

## STAR★METHODS

### KEY RESOURCES TABLE

REAGENT or RESOURCE	SOURCE	IDENTIFIER
<b>Antibodies</b>		
Total OXPHOS Rodent (4.5 μg/ml)	Abcam	Cat. #ab110413; RRID: AB_2629281
Rabbit anti-Hemopexin (1:1000)	Abcam	Cat. #ab133415; RRID: AB_2890603
Rabbit anti-Heme Oxygenase-1 (1:1000)	Abcam	Cat. #ab13243; RRID: AB_299790
Rabbit anti-Gapdh (1:1000)	Abcam	Cat. #ab9485; RRID: AB_307275
Mouse anti-Heme Oxygenase 2 (1:1000)	Santa Cruz Biotechnology	Cat. #sc17786; RRID: AB_627728
Anti-Myosin I (1:200)	Developmental Studies Hybridoma Bank	Cat. #BA-D5; RRID: AB_2235587
Anti-Myosin IIA (1:200)	Developmental Studies Hybridoma Bank	Cat. #SC-71; RRID: AB_2147165
Anti-Myosin IIB (1:200)	Developmental Studies Hybridoma Bank	Cat. #BF-F3; RRID: AB_2266724
Rabbit anti-Laminin (1:300)	Sigma-Aldrich	Cat. #L9393; RRID: AB_477163
Rabbit anti-OPA1 (1:1000)	Cell Signaling	Cat. #80471; RRID: AB_2734117
Rabbit anti-MTFN1 (1:1000)	Cell Signaling	Cat. #14739; RRID: AB_2744531
Rabbit anti-MTFN2 (1:1000)	Cell Signaling	Cat. #9482; RRID: AB_2716838
Rabbit anti-DRP1 (1:1000)	Cell Signaling	Cat. #5391; RRID: AB_11178938
Alexa Fluor 488 goat anti-Mouse IgG1 (1:200)	ThermoFisher Scientific	Cat. #a21121; RRID: AB_2535764
AlexaFluor 594 Goat anti-Mouse IgM (1:200)	ThermoFisher Scientific	Cat. #a21044; RRID: AB_2535713
Cy5 Goat anti-Rabbit IgG (1:200)	ThermoFisher Scientific	Cat. #a10523; RRID: AB_2534032
800CW Goat anti-Mouse IgG (1:20000)	Li-Cor	Cat. #926-32210; RRID: AB_2687825
800CW Goat anti-Rabbit IgG (1:20000)	Li-Cor	Cat. #926-32211; RRID: AB_2651127
680RD Goat anti-Mouse IgG (1:20000)	Li-Cor	Cat. #926-68070; RRID: AB_2651128
680RD Goat anti-Rabbit IgG (1:20000)	Li-Cor	Cat. #926-68071; RRID: AB_2721181
<b>Chemicals, peptides, and recombinant proteins</b>		
Glutamic acid	Sigma-Aldrich	Cat. #G1251
Adenosine 5'-diphosphate	Sigma-Aldrich	Cat. #A2754
Osmium tetroxide	Ted-Pella, Inc.	Cat. #20816-12-0
Uranyl Acetate	Ted-Pella, Inc.	Cat. #19481
Lipofectamine RNAiMAX	ThermoFisher Scientific	Cat. #13778030
SYBR Green Master Mix	ThermoFisher Scientific	Cat. #A25742
Human plasma Hemopexin	Athens Research & Technology	Cat. #16-16-080513
Hemin	Sigma-Aldrich	Cat. #51280
Protease inhibitor cocktail	ThermoFisher Scientific	Cat. #78430
Malic acid	Sigma-Aldrich	Cat. #M1000
Mouse-on-Mouse blocking reagent	Vector Laboratories	Cat. #MKB-2213-1
F-10 nutrient mix	ThermoFisher Scientific	Cat. #11550043
Horse serum	ThermoFisher Scientific	Cat. #26050
Collagenase/Dispase Blend I	Millipore	Cat. #scr139
Rat Tail Collagen I	ThermoFisher Scientific	Cat. #A1048301
Fetal bovine serum	Sigma-Aldrich	Cat. #F7524
Basic fibroblast growth factor (bFGF)	ThermoFisher Scientific	Cat.#13256-029
<b>Critical commercial assays</b>		
Mouse Hemopexin Elisa kit	Novus Biologicals	Cat. #NBP2-60633
Citrate Synthase Activity Assay Kit	Cayman Chemical	Cat. #701040
Mito Stress Test Kit	Agilent	Cat. #103010-100

(Continued on next page)

<b>Continued</b>		
REAGENT or RESOURCE	SOURCE	IDENTIFIER
High-Capacity cDNA Kit	ThermoFisher Scientific	Cat. #4368814
Creatine kinase	IDEXX Laboratories	Cat. #6212
Lactato dehydrogenase	IDEXX Laboratories	Cat. #6218
Lipid Peroxidation Assay Kit	Abcam	Cat. #ab118970
Cell Counting Kit-8	Dojindo Molecular Technologies, Inc.	Cat. #CK04-05
Hemin Assay Kit	GenWay Biotech Inc.	Cat. #GWB-AXR320
<b>Experimental models: Cell lines</b>		
Primary Muscle Satellite Cells (PMC)	This paper	N/A
<b>Experimental models: Organisms/strains</b>		
Mouse: B6.129- <i>Hpx<sup>tm1Altr</sup>/J</i>	The Jackson Laboratory	JAX stock#029380
Mouse: HSA-MerCreMer	The Jackson Laboratory	JAX stock#025750
Mouse: <i>Hmox1<sup>fl/fl</sup></i>	RIKEN BioResource Center	Cat. #RBRC03163
Mouse: HSA-MCM-Cre- <i>Hmox1<sup>fl/fl</sup></i>	This paper	N/A
Mouse: C57BL/6	Charles River Laboratories	NCI stock# 556
Rat: LCR and HCR	The University of Toledo, OH, USA	<a href="https://www.utoledo.edu/med/depts/physpharm/ExerciseRatResources.html">https://www.utoledo.edu/med/depts/physpharm/ExerciseRatResources.html</a>
<b>Oligonucleotides</b>		
siHmox1	ThermoFisher Scientific	Cat. #s67607
siHpx	ThermoFisher Scientific	Cat. #s67790
RT-qPCR mRNA	See <a href="#">Table S1</a> for oligonucleotide information	N/A
<b>Software and algorithms</b>		
SMASH	<a href="#">Smith and Barton, 2014</a>	<a href="https://dx.doi.org/10.6084/m9.figshare.1247634">https://dx.doi.org/10.6084/m9.figshare.1247634</a>
ImageJ	<a href="#">Schneider et al., 2012</a>	<a href="https://imagej.nih.gov/ij/">https://imagej.nih.gov/ij/</a>
DataAssist	ThermoFisher Scientific	N/A
GNU Image Manipulation Program (GIMP)	GNU	<a href="https://www.gimp.org">https://www.gimp.org</a>
Prism 6	GraphPad	<a href="https://www.graphpad.com">https://www.graphpad.com</a>
Primer-Blast	NCBI	<a href="https://www.ncbi.nlm.nih.gov/tools/primer-blast">https://www.ncbi.nlm.nih.gov/tools/primer-blast</a>
<b>Other</b>		
Animal Treadmill: Exer 3/6	Columbus Instruments	Cat. #1055-SRM
Rota-Rod	Med Associates Inc	Cat. #ENV-571M
Resource website for images creation	This paper	<a href="https://biorender.com/">https://biorender.com/</a>

## RESOURCE AVAILABILITY

### Lead contact

Further information and requests for resources and reagents should be directed to and will be fulfilled by the Lead Contact, Leo E. Otterbein (Department of Surgery, Beth Israel Deaconess Medical Center, Harvard Medical School, [lotterbe@bidmc.harvard.edu](mailto:lotterbe@bidmc.harvard.edu)).

### Materials availability

This study did not generate any unique reagents.

### Data and code availability

This study did not generate/analyze datasets/code.

## EXPERIMENTAL MODEL AND SUBJECT DETAILS

For cell lines, primary satellite cells were isolated and cultured from the entire hind limb of wild-type/control (WT) mice as previously described ([Megeney et al., 1996](#)). Briefly, muscles were dissected and digested in collagenase/dispase solution (Millipore) for 30min

at 37°C. Cells were initially plated on non-coated plates and incubated for 30 min at 37°C to remove the fibroblast excess. Next, cells were plated onto dishes coated in rat tail collagen I (GIBCO) and cultured in plating medium for up to several days in growth medium containing Ham's F-10 nutrient mixture (GIBCO), 20% fetal bovine serum (Sigma), 2.5 ng/ml basic fibroblast growth factor (bFGF, Invitrogen), with streptomycin and penicillin (GIBCO) at 37°C in 5% CO<sub>2</sub>. For experiments where cells were differentiated, cells were plated on collagen-coated dishes and grown until 50% confluent. At that time, growth medium was exchanged for differentiation medium containing DMEM, 5% horse serum, and antibiotics. Cells were differentiated for 72 hours, transfected and analyzed.

For *in vivo* animal studies, isogenic male mice C57BL/6 (Wild-type, WT), Hemopexin (*Hpx*<sup>-/-</sup>, # 029380) and HSA-Cre transgenic mice (# 025750) were purchased from Charles River or Jackson Laboratory (25–30 g). Skeletal muscle-specific HO-1 knockout (*tamoxifen-HSA-MCM-Cre-Hmox1<sup>fl/fl</sup>*) was achieved by breeding *Hmox1<sup>fl/fl</sup>* mice (Riken Bio Resource Center, Stock-# RBRC03163) with mice expressing Cre recombinase under the actin alpha-1, skeletal muscle (Jackson Laboratory, Stock-# 025750). To selectively delete skeletal muscle *Hmox1* gene HSA-MCM-Cre-*Hmox1<sup>fl/fl</sup>* 8- to 10-week-old mice were fed a chow containing 400 mg tamoxifen for one month. HCR and LCR twelve weeks old rats from the 32<sup>o</sup> generation were used (Koch and Britton, 2001; Wisløff et al., 2005). The heart (ventricle), tibialis anterior, extensor digitorum longus, soleus, plantaris, and gastrocnemius muscles were carefully harvested from animal's hind-limb and stored in -80°C. All mouse and rat procedures were approved by the Beth Israel Deaconess Medical Center (BIDMC) Institutional Animal Care and Use Committee (IACUC, #032-2018), Norwegian Council for Animal Research (#5243), and University of São Paulo Ethical Committee (#2015/02) were in accordance with the Association for the Assessment and Accreditation of Laboratory Animal Care guidelines.

## METHOD DETAILS

### Graded treadmill exercise test and aerobic exercise protocols

All animals were acclimatized to a treadmill (Exer 3/6, Columbus Instruments, USA) over four consecutive days, 10 min/day at 6 m/min. After the acclimatization period, animals were subjected to a graded maximal exhaustive test. The test started at 6 m/min and speed was increased by 3 m/min every 3 minutes until mice were unable to run due to exhaustion (Ferreira et al., 2007). Tests were carried out by a single observer (RWAS), blinded to mouse identity. Total distance run (meters) and peak workload (m/min) were recorded. After that, mice were subjected to an acute moderate-intensity aerobic exercise bout for 90 min or six weeks, five days/week at 60% of maximal workload achieved in a graded treadmill running test described above, corresponding to maximal lactate steady state (Ferreira et al., 2007). After acute exercise, samples were collected at different time points (immediately after, 3, 6, and 24 h). For the running training protocol, at the end of the third training week, animals were reevaluated for running performance in order to adjust running speed intensity. All samples were carefully harvested at 72 hours after the end of the training protocol.

### Rotarod performance

Motor function was assessed by habituating mice to the Rotarod (Single Station Rota-Rod Treadmill, Med Associated Inc., USA) for 1 week, at different rotation speeds in 5 min-long sessions. The speed was gradually increased from 4 to 40 rpm over a period of 5 min, and the time that the mice spent on the rod was recorded. Three successive trials were performed, and the best individual performances were considered for further analysis.

### Mitochondrial isolation and activity

Skeletal muscle mitochondria isolation and function were assessed as previously described (60, 61). Briefly, muscle samples from gastrocnemius were minced and homogenized in isolation buffer to release mitochondria from within muscle fibers and washed in the same buffer in the presence of 1 mg/mL bovine serum albumin. The suspension was homogenized and centrifuged. The resulting supernatant was centrifuged at higher speed for 10 min. The mitochondrial pellet was washed, resuspended in isolation buffer and submitted to a new centrifugation. The mitochondrial pellet was washed, and the final pellet was resuspended in a minimal volume of isolation buffer to be subjected to the functional assay. The experiments with isolated mitochondria (10 μg mitochondrial protein/mL) were monitored in experimental buffer and were made in the presence of malate (Sigma, M1000) and glutamate (Sigma, G1251) substrates (2 mM of each). Oxygen consumption rate (OCR) was measured using a XFp extracellular flux analyzer. Ten-microgram/well of isolated mitochondria in experimental buffer was seeded in a plate and centrifuged. Each well was filled up to 180 μL with assay buffer in the presence of glutamate (5 mM) and malate (5 mM), as substrates. ADP (4 mM, Sigma 2754) was added to induce state 3 respiratory rates. Subsequent addition of oligomycin (2 μM) was used to determine state 4 rates. Respiratory control ratios were calculated by the ratio of state 3: state 4. Additionally, 2 μM carbonyl cyanide 4-(trifluoromethoxy) phenylhydrazone (FCCP) was added to evaluate O<sub>2</sub> consumption during the mitochondrial uncoupling state. All other procedures were performed according to manufacturer's instructions (Agilent Seahorse, XF cell Mito stress kit).

### Heme and hemopexin content

Serum (DIHM-250, BioAssay Systems; GWB-AXR320, Genway Biotech Inc) and tissue (GWB-AXR320, Genway Biotech Inc) concentrations of heme were determined colorimetrically according to the manufacturer's instructions. Hpx were determined by ELISA (NBP2-60633, Novusbio) according to the manufacturer's instructions.

### Biochemical analyses

Lipid peroxidation and citrate synthase activity were determined colorimetrically in the muscle cells and plantaris according to the manufacturer's instructions, respectively (ab118970, Abcam; 701040, Cayman Chemical, USA).

### Quantitative real-time PCR

Total RNA was extracted from cells and tissues using TRizol reagent (Invitrogen) following manufacturer's instruction. Reverse transcription was performed using High-Capacity cDNA synthesis kit (ThermoFisher Scientific). After cDNA synthesis, quantitative real-time PCR for target and endogenous genes (Table S1) ran separately, and amplifications were detected with a StepOne Plus (Applied Biosystems, Foster City, CA, USA) by using PowerUp SYBR Green Master Mix (ThermoFisher Scientific). Spleen, liver, and heart expression levels were normalized to  $\beta$ -actin (Actb), while soleus and plantaris were normalized to Hprt1. Fold-change was calculated through  $\Delta\Delta C_t$  method.

### Immunoblotting

Protein extraction, quantification, preparation and immunoblotting experiments were performed as previously described (Souza et al., 2018). Briefly, tissue samples were homogenized in RIPA lysis buffer (50 mM Tris/HCl, pH 8.0, 150 mM NaCl, 1% NP-40, and 0.1% SDS) containing HALT Protease and Phosphatase inhibitor cocktail solution (ThermoFisher Scientific). After homogenization, tissue lysates were incubated on ice for 30min. Samples were centrifuged at 14,000 g for 20 min at 4°C. The supernatant was collected, and protein estimation was performed using Pierce BCA Protein Assay Kit (Thermo Scientific, Rockford, IL) before Laemmli sample buffer containing 2-Mercaptoethanol (BioRad) was added. 30 mg of total protein lysate was resolved on SDS polyacrylamide gel according to standard procedure at 20 mA per gel and blotted onto a nitrocellulose membrane 0.45 mm (GE Healthcare) via Mini Trans-blot module (Bio-Rad) at a constant voltage (100 V) for 2 h. After blocking with 5% non-fat milk (Serva)/Tris-buffered saline with 0.05% Tween 20 (TBS-T) for 1 h, the membrane was incubated overnight in 5% bovine serum albumin (Sigma)/TBS-T with primary antibody against mitochondrial OXPHOS (ab110413, Abcam), Hpx (ab133415, Abcam), Hmox1 (ab13243, Abcam), Hmox2 (sc17786, Santa Cruz), Mitofusin-1 (#14739, Cell Signaling), Mitofusin-2 (#9482, Cell Signaling), Opa-1 (#80471, Cell Signaling), Drp-1 (#5391, Cell Signaling) and Gapdh (ab9485, Abcam). Secondary specific antibodies were goat anti-mouse IR800 and goat anti-rabbit IR680 and IR800 (LICOR). Membranes were scanned using the Odyssey infrared imaging system (LICOR).

### Cell culture

Cells were differentiated into myotubes using DMEM containing 5% horse serum for 72h. Cells were transfected (RNAiMAX) with siRNA duplexes targeting HO-1 (s67607), Hpx (s67790) or scrambled control siRNA (100 pmol, Thermo Fisher Scientific). PMC with the gene targets silenced or not were subjected to heme (10  $\mu$ M, 50  $\mu$ M and 100  $\mu$ M), and hemopexin (1  $\mu$ M) interventions. After 24h, cell viability was measured by Cell Counting Kit-8 (CCK-8) according to the manufacturer's instructions (Dojindo, Japan).

### Analysis of skeletal muscle damage

Serum creatine kinase (CK) and lactate dehydrogenase (LDH) were used for evaluation of muscle damage. Blood samples were collected at the indicated time points from the heart, immediately before induced death. Serum samples were analyzed on an IDEXX Catalyst DX analyzer (IDEXX Laboratories).

### Histological analysis

Tibialis anterior were dissected, embedded in OCT compound and flash-frozen in liquid nitrogen. Muscle cryosections (10  $\mu$ m) were subjected to hematoxylin and eosin (H&E) staining using a standard protocol. Moreover, immunohistochemical staining for Succinate dehydrogenase (SDH) activity was determined as general indices of oxidative potential and was performed as previously described (Blanco et al., 1988). Immunofluorescence was performed with the following antibodies: anti-myosin I (BA-D5), anti-myosin IIA (SC-71) and anti-myosin IIB (BF-F3) (Developmental Studies Hybridoma Bank). Skeletal muscle cell membrane was stained for laminin (Sigma). Labeling of cryosections with mouse monoclonal primary antibodies was performed using the fluorescein M.O.M kit staining (Vector Laboratories) according to the manufacturer's instructions. For immunofluorescence, secondary antibodies were coupled to Alexa-405, Alexa 488, Alexa-594 or Alexa-647 fluorochromes, and nuclei were stained with DAPI (Invitrogen). After washing, tissue sections were mounted with Mowiol. Morphometric analyses were made in whole muscles at 10X magnification and images were captured with Revolve R4 fluorescence microscopy (Echo app, Echo Laboratories). Fiber frequency was analyzed using ImageJ software and muscle fiber cross-sectional area was measured using a freely and open-source software SMASH-Semiautomatic Image Processing of Skeletal Muscle Histology (Smith and Barton, 2014). All histological analyses were conducted by a single observer (RWAS) blinded to mouse identity.

### Transmission electron microscopy

The extensor digitorum longus muscle was excised and fixed under tension in modified Karnovsky fixative containing 2.5% glutaraldehyde (Electron Microscopy and Sciences, Hatfield, PA) and 2.5% formaldehyde (EMS) in sodium cacodylate (Sigma-Aldrich) buffer, pH 7.4. Tissues were fixed for 1h at room temperature and then cut in fixative lengthwise into 300  $\mu$ m length x 300  $\mu$ m height tissue pieces. Tissues were washed with cacodylate buffer and then transferred to a 300  $\mu$ m deep aluminum planchette (Technotrade

Int., Manchester, NH). The planchette was filled with 20% BSA (Sigma-Aldrich) in Gomori phosphate buffer, pH 7.4 containing 5% FBS (GIBCO/ThermoFisher), capped, and the tissue frozen in a Wolwhend Compact 02 High Pressure Freezer (Technotrade Int.). The frozen tissues were embedded in LX112 resin (Ladd Research, Williston, VT) after super-quick freeze substitution (Reference, below) in 1% osmium tetroxide (Ted Pella Inc., Redding, CA), 0.1% uranyl acetate (Ted Pella), and 5% dH<sub>2</sub>O in acetone. Sections were cut using an Ultracut E Ultramicrotome (Leica Microsystems, Buffalo Grove, IL), placed on formvar and carbon-coated slot grids, and examined in a JEOL 1400 electron microscope (JEOL, Peabody, MA) outfitted with Orius CCD cameras (Gatan, Pleasanton, CA). Digital Micrograph software (Gatan) was used to collect digital images.

#### QUANTIFICATION AND STATISTICAL ANALYSIS

Statistical analysis was conducted using GraphPad Prism 6 software and the values are expressed at means  $\pm$  SEM. Statistical analyses were performed using the Student's t test and one or two-way ANOVA with post hoc application of the Tukey test to adjust for multiple comparisons when appropriate. P values less than 0.05 were considered significant.